



King's Research Portal

DOI:

[10.1242/dev.176776](https://doi.org/10.1242/dev.176776)

Document Version

Publisher's PDF, also known as Version of record

[Link to publication record in King's Research Portal](#)

Citation for published version (APA):

Crespo-Enriquez, I., Hodgson, T., Zakaria, S., Cadoni, E., Shah, M., Allen, S., Al-Khishali, A., Mao, Y., Yiu, A., Petzold, J., Villagomez-Olea, G., Pitsillides, A. A., Irvine, K. D., & Francis-West, P. (2019). Dchs1-fat4 regulation of osteogenic differentiation in mouse. *Development (Cambridge)*, 146(14), Article dev176776 .
<https://doi.org/10.1242/dev.176776>

Citing this paper

Please note that where the full-text provided on King's Research Portal is the Author Accepted Manuscript or Post-Print version this may differ from the final Published version. If citing, it is advised that you check and use the publisher's definitive version for pagination, volume/issue, and date of publication details. And where the final published version is provided on the Research Portal, if citing you are again advised to check the publisher's website for any subsequent corrections.

General rights

Copyright and moral rights for the publications made accessible in the Research Portal are retained by the authors and/or other copyright owners and it is a condition of accessing publications that users recognize and abide by the legal requirements associated with these rights.

- Users may download and print one copy of any publication from the Research Portal for the purpose of private study or research.
- You may not further distribute the material or use it for any profit-making activity or commercial gain
- You may freely distribute the URL identifying the publication in the Research Portal

Take down policy

If you believe that this document breaches copyright please contact librarypure@kcl.ac.uk providing details, and we will remove access to the work immediately and investigate your claim.

RESEARCH ARTICLE

Dchs1-Fat4 regulation of osteogenic differentiation in mouse

Ivan Crespo-Enriquez¹, Tina Hodgson^{1,*}, Sana Zakaria^{1,*}, Erika Cadoni¹, Mittal Shah², Stephen Allen², Ayman Al-Khishali¹, Yaopan Mao³, Angela Yiu¹, Jonna Petzold¹, Guillermo Villagomez-Olea¹, Andrew A. Pitsillides², Kenneth D. Irvine³ and Philippa Francis-West[‡]

ABSTRACT

In human, mutations of the protocadherins FAT4 and DCHS1 result in Van Maldergem syndrome, which is characterised, in part, by craniofacial abnormalities. Here, we analyse the role of Dchs1-Fat4 signalling during osteoblast differentiation in mouse. We show that *Fat4* and *Dchs1* mutants mimic the craniofacial phenotype of the human syndrome and that Dchs1-Fat4 signalling is essential for osteoblast differentiation. In *Dchs1/Fat4* mutants, proliferation of osteoprogenitors is increased and osteoblast differentiation is delayed. We show that loss of Dchs1-Fat4 signalling is linked to increased Yap-Tead activity and that Yap is expressed and required for proliferation in osteoprogenitors. In contrast, Taz is expressed in more-committed Runx2-expressing osteoblasts, Taz does not regulate osteoblast proliferation and Taz-Tead activity is unaffected in *Dchs1/Fat4* mutants. Finally, we show that Yap and Taz differentially regulate the transcriptional activity of Runx2, and that the activity of Yap-Runx2 and Taz-Runx2 complexes is altered in *Dchs1/Fat4* mutant osteoblasts. In conclusion, these data identify Dchs1-Fat4 as a signalling pathway in osteoblast differentiation, reveal its crucial role within the early Runx2 progenitors, and identify distinct requirements for Yap and Taz during osteoblast differentiation.

KEY WORDS: Dchs1-Fat4, Yap/Taz, Runx2, Osteoblast

INTRODUCTION

How signalling networks integrate to control osteoblast proliferation and differentiation to form bone during embryonic development and postnatally is a fundamental question. Bones are not only essential for locomotion but provide support and protection of internal structures and play crucial roles in many aspects of physiology. Bones are reservoirs for phosphorous and calcium, are important for glucose metabolism, house the haematopoietic system and are essential for the function of the renal and male reproductive systems. Bone is continually remodelled throughout life and de-regulation can result in bone disorders such as osteoporosis, the most frequent bone disorder contributing to significant morbidity in the elderly. Osteogenic differentiation is initiated within mesenchymal or endochondral precursors through the expression of the transcription factor Runx2, which is essential for osteoblast

differentiation (Komori et al., 1997; Otto et al., 1997). Runx2 directly regulates the expression of the transcription factor osterix (Sp7), the cell cycle inhibitor p21 (Cdkn1a), alkaline phosphatase, and the matrix protein Bglap (bone γ -carboxyglutamate protein, also known as osteocalcin), to control cell differentiation along the osteogenic pathway (Westendorf et al., 2002).

Recently, loss-of-function mutations in the protocadherins DCHS1 and FAT4 have been shown to be responsible for Van Maldergem syndrome, which is, in part, characterised by craniofacial defects including enlarged fontanelles and underdevelopment of the maxilla (Cappello et al., 2013; Mansour et al., 2012; Neuhann et al., 2012; Zampino et al., 1994). In some patients, a generalised osteopenia has also been reported (Mansour et al., 2012). Dchs1 and Fat4 typically act as a ligand-receptor pair (Mao et al., 2011, 2015, 2016; Zakaria et al., 2014; Bagherie-Lachidan et al., 2015) and this new data indicates that they may be crucial for the maintenance of skeletal integrity in humans and potentially identifies a new signalling pathway in osteogenic differentiation.


Ds and Fat, the *Drosophila* homologues of vertebrate Dchs1 and Fat4, respectively, have two key functions during development: they inhibit tissue growth and regulate planar cell polarity (PCP), the coordinated polarised cell behaviour within a plane of a tissue (Matis and Axelrod, 2013; Irvine and Harvey, 2015). Examples of PCP include the polarised orientation of cellular structures, such as the bristles and hairs on the *Drosophila* wing and abdomen. Fat and Ds inhibit tissue growth via inhibition of the Hippo pathway, which regulates the activity of the Yorkie/Scalloped transcriptional complex to control cell proliferation, survival and differentiation (Misra and Irvine, 2018). In the absence of Fat/Ds, Yorkie signalling is increased resulting in overgrowth and dysplasia of the imaginal discs.

There is now clear evidence for conservation of Dchs1-Fat4 regulation of PCP in vertebrates. In mice, Dchs1-Fat4 regulates PCP ensuring orientated and collective cell behaviours during elongation of the developing kidney tubules, development of the sternum and migration of the facial branchiomotor neurons (Saburi et al., 2008; Mao et al., 2016; Zakaria et al., 2014). There is also evidence in vertebrates for regulation of the Yorkie homologues, Yap (YES-associated protein; Yap1) and Taz (transcriptional coactivator with PDZ-binding motif; Wwtr1). Loss of Dchs1-Fat4 signalling in the developing mouse cerebral cortex and heart results in increased proliferation that can be rescued by downregulation of Yap (Cappello et al., 2013; Ragni et al., 2017). Similarly, loss of Fat4 in the chick neural tube results in decreased phosphorylation of Yap (pYap), the inactive form of Yap, together with increased proliferation of a subset of neurons, again implicating loss of Fat4 signalling with activation of Yap (Van Hateren et al., 2011). In the mouse kidney, Fat4 regulation of Yap/Taz intracellular localisation within nephrogenic precursors has also been observed by some (Das et al., 2013) but not by other researchers (Bagherie-Lachidan et al., 2015; Mao et al., 2015).

¹Centre for Craniofacial and Regenerative Biology, Faculty of Dentistry, Oral & Craniofacial Sciences, King's College London, Floor 27, Guy's Tower, London SE1 9RT, UK. ²Comparative Biomedical Sciences, Royal Veterinary College, Camden, London, NW1 0TU, UK. ³Waksman Institute and Department of Molecular Biology and Biochemistry, Rutgers University, Piscataway, NJ 08854, USA.

*These authors contributed equally to this work

[‡]Author for correspondence (philippa.francis-west@kcl.ac.uk)

 I.C.-E., 0000-0003-2967-4554; P.F.-W., 0000-0001-5179-5892

Both PCP and Yap/Taz have been implicated in osteogenic development. The Fz-PCP pathway controls the orientation of cell divisions in the osteoblastic cell line Saos-2 (Galea et al., 2015), and Yap/Taz can modulate the activity of Runx2. Specifically, it has been shown that Taz can potentiate the activity of the osteoblast determination transcription factor Runx2 to promote osteoblast differentiation, and inhibit expression of PPAR γ , which controls adipocyte fate (Cui et al., 2003; Hong et al., 2005; Pan et al., 2018). In contrast, Yap can inhibit the ability of Runx2 to activate specific transcriptional targets such as TGF β receptor type 1 and the matrix protein Bglap (Zaidi et al., 2004). Activation of Yap/Taz in response to mechanotransduction signals induced by the actin cytoskeleton and matrix stiffness also promotes osteoblast differentiation from mesenchymal stem cells (Dupont et al., 2011).

Here, using genetic mouse models, we determine the function, and mechanisms of action, of Dchs1-Fat4 signalling during osteogenic development and identify a new signalling pathway that is required intrinsically during osteoblast differentiation. We show that *Dchs1* and *Fat4* mouse mutants are characterised by an under-development of the cranial skeletal structures, as in Van Maldergem patients. We show that one of the key roles of Dchs1-Fat4 signalling is within the early Runx2-positive (Runx2^{+ve}) osteogenic progenitors – in the absence of either Dchs1 or Fat4, proliferation is increased and this is coupled with delayed progression along the differentiation pathway. *In vitro* analysis revealed that this is linked with increased activity of Yap-Tead, but not Taz-Tead, activity. Additionally, loss of Dchs1-Fat4 signalling results in increased activity of the Runx2-TGF β R1 reporter and

decreased activity of the generic Runx2 and Runx2-p21 reporters, which we show are differentially regulated by Yap and Taz.

RESULTS

Defective skeletal development in *Dchs1* and *Fat4* mutants

Van Maldergem syndrome patients are characterised by pronounced craniofacial skeletal defects including enlarged fontanelles (Zampino et al., 1994). To determine potential roles of Fat4 and Dchs1 during skeletogenesis, wild-type, heterozygous, *Fat4*^{-/-} and *Dchs1*^{-/-} postnatal day (P) 0 mice were first analysed by micro-computed tomography (μ -CT) imaging and Alizarin Red/Alcian Blue staining to identify alterations in skeletal development. The size of different bones, specifically the mandible, frontal, parietal, interparietal and palatine bones, within the craniofacial complex was also determined.

This analysis revealed that all craniofacial bones are specified appropriately but all bones analysed are significantly smaller in *Dchs1*^{-/-} and *Fat4*^{-/-} mutants (Fig. 1; Fig. S1A; Tables S1, S2; *Dchs1*^{+/+} *n*=3, *Dchs1*^{-/-} *n*=4, *P*<0.01; *Fat4*^{+/+} *n*=3, *Fat4*^{-/-} *n*=3, *P*<0.01). Thus, the face is smaller and the cranial vault is characterised by larger fontanelles (Fig. 1A, Fig. S1A). This is not due to a developmental delay as the body and head size of *Fat4*^{-/-} and *Dchs1*^{-/-} mutants are not significantly different from their heterozygous and wild-type littermates (Mao et al., 2011). Both neural crest-derived (frontal, mandible, palatine) and mesodermally derived (parietal and interparietal) bones are affected, indicating that the decreased ossification is not related to tissue origin. Heterozygous mice had no overt phenotype (Fig. S1A,B; Table S2; *Dchs1*^{+/-} *n*=4,

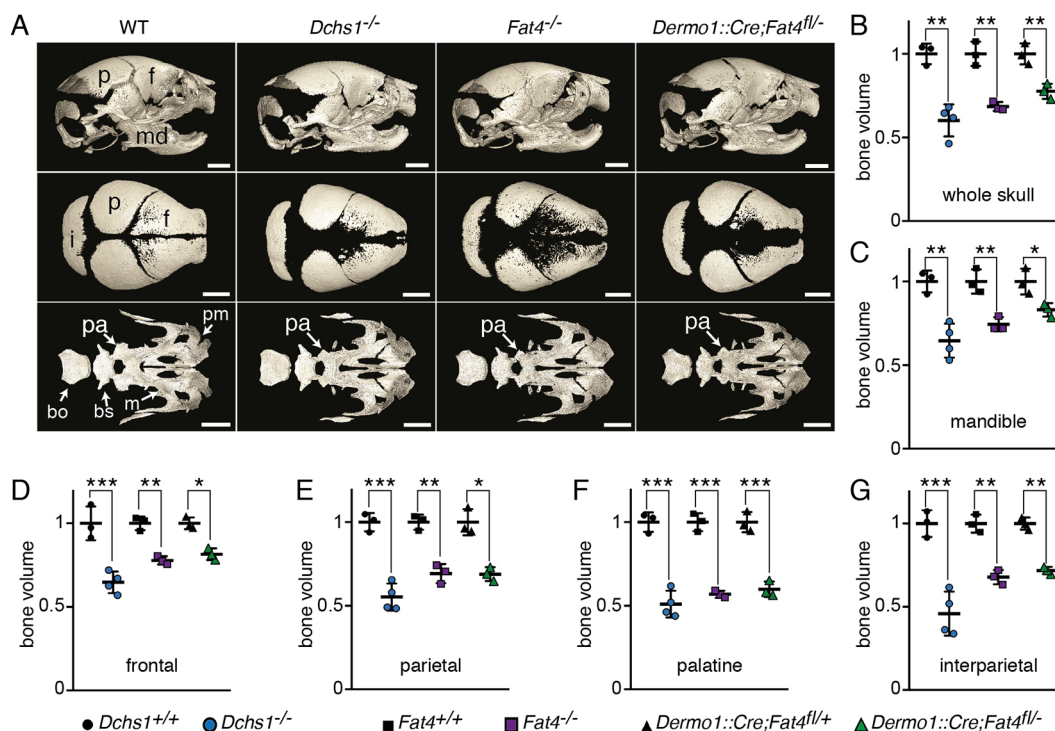


Fig. 1. *Dchs1* and *Fat4* are required for cranial skeletal development. (A) μ -CT scans of wild-type (WT; *Dchs1*^{+/+} *n*=3; *Fat4*^{+/+} *n*=3), *Dchs1*^{-/-} (*n*=4), *Fat4*^{-/-} (*n*=3), *Dermo1*^{Cre}; *Fat4*^{fl/-} (*n*=3) P0 pups. The control *Dermo1*^{Cre}; *Fat4*^{fl/+} (*n*=3), which have no phenotype, are not shown. The upper row shows sagittal views of the skull and face, the middle row shows the skull cap and the lower row shows the cranial base and upper jaw. (B-G) Quantification of the relative size of the skull cap (B) and individual bones (C-G) in *Dchs1*^{-/-}, *Fat4*^{-/-} and *Dermo1*^{Cre}; *Fat4*^{fl/-} mutants compared with their wild-type and control *Dermo1*^{Cre}; *Fat4*^{fl/+} littermates, respectively. Within each control group (wild type and control *Dermo1*^{Cre}; *Fat4*^{fl/+}) the average measurement was standardised to 1. In some CT images, background 'noise/dots' between the bones in the CT scans may have been removed for clarity. bo, basioccipital; bs, basisphenoid; f, frontal; i, interparietal; m, maxilla; md, mandible; p, parietal; pa, palatine; pm, premaxilla bones. Unpaired two-tailed Student's *t*-test: **P*<0.05; ***P*<0.01; ****P*<0.001. Error bars represent s.e.m. Scale bars: 1 mm.

Fat4^{+/-} *n*=4). Quantification of the bone mineral density within the frontal, parietal and interparietal bones revealed no significant difference in *Dchs1*^{-/-} and *Fat4*^{-/-} mutants compared with wild-type controls (Fig. S1C; Tables S3, S4; *Dchs1*^{-/-} *n*=4, *Fat4*^{-/-} *n*=3). Alizarin Red and Alcian Blue staining revealed that *Fat4*^{-/-}/*Dchs1*^{-/-} double mutant mice had palatine and mandible defects that were identical to those of the *Fat4*^{-/-} and *Dchs1*^{-/-} single mutants, suggesting that they act as a dedicated receptor-ligand pair as in many other regions of the embryo (Fig. S1D; *n*=3; Mao et al., 2011).

To exclude the possibility that changes in craniofacial bone development are secondary to alterations in development of soft tissues such as the eye, brain and skeletal muscle, *Dermo1*^{Cre/+}; *Fat4*^{fl/-}, *Dermo1*^{Cre/+}; *Dchs1*^{fl/-} and *Mesp1*^{Cre/+}; *Dchs1*^{fl/fl} mice were generated. In the *Dermo1*^{Cre} lines, *Fat4* and *Dchs1* expression are silenced in both the mesodermal- and neural crest-derived pre-osteoblast progenitors whereas in *Mesp1*^{Cre/+}; *Dchs1*^{fl/fl} mice, *Dchs1* is silenced in the mesoderm that gives rise to the parietal and part of the interparietal bone. We found that in *Dermo1*^{Cre/+}; *Fat4*^{fl/-} and *Dermo1*^{Cre/+}; *Dchs1*^{fl/-} mice there is a significant reduction in the size of all the craniofacial bones analysed (Fig. 1; Fig. S1E; Tables S1, S2, S8; *Dermo1*^{Cre/+}; *Fat4*^{fl/-} *n*=3, *P*<0.05; *Dermo1*^{Cre/+}; *Dchs1*^{fl/-} *n*=3, *P*<0.005). Likewise, in P0 *Mesp1*^{Cre/+}; *Dchs1*^{fl/fl} mice, there was a significant reduction in the size of the parietal and interparietal bones where the Cre-recombinase is expressed, compared with control mice (Fig. S1F; Table S5; *Mesp1*^{Cre/+}; *Dchs1*^{fl/fl} *n*=3, *P*<0.01). As internal controls in P0 *Mesp1*^{Cre/+}; *Dchs1*^{fl/fl} mice, the neural crest-derived palatine and frontal bones, where the Cre-recombinase is not expressed, were also analysed. As would be expected, these bones were not affected (Fig. S1F).

As Van Maldergem patients show a generalised osteopenia, the appendicular skeleton, which develops via endochondral ossification, was also examined. Analysis of the femur revealed that there is a decrease in several bone parameters [BV/TV (mineralised bone volume/total bone volume), trabeculae number, cortical thickness] in *Dchs1*^{-/-} mutants (Fig. 2; Table S6; *Dchs1*^{+/+} *n*=5, *Dchs1*^{-/-} *n*=7; BV/TV *P*<0.05; trabeculae number *P*<0.05; cortical thickness-midshaft, *P*<0.05; cortical thickness-metaphysis *P*<0.05). In contrast, in *Fat4*^{-/-} mutants, there was only a significant decrease in cortical thickness at the midshaft (Fig. 2; Table S6;

Fat4^{+/+} *n*=5, *Fat4*^{-/-} *n*=5, *P*<0.01). Therefore, the bone defects in *Dchs1*^{-/-} and *Fat4*^{-/-} mutants also encompass at least some aspects of endochondral bone development.

Dchs1-Fat4 function in the osteoblast progenitors

To analyse bone development further in *Dchs1*^{-/-} and *Fat4*^{-/-} mutants, we next determined when the craniofacial skeletal abnormalities are detectable, and then determined which osteogenic cell populations express *Dchs1* and *Fat4* at these stages of development.

Alizarin Red and Alcian Blue staining of embryonic day (E) 15.5 and E16.5 *Dchs1* mutant embryos revealed that the mandible and palatine bones are visibly smaller at E15.5 and E16.5, respectively (Fig. 3). Thus, the defects start to arise during the very early phases of bone development. *In situ* hybridisation analysis at these stages revealed that *Fat4* and *Dchs1* are expressed in both the osteoblast precursors and within the more differentiated osteoblasts (Fig. 4A).

To determine whether osteoblast differentiation is altered, the expression of the osteogenic markers Runx2, osterix, osteopontin (Spp1) and Bglap, which characterise different stages of osteoblast differentiation, were analysed in tissue sections through the developing palatine and calvaria bones at E15.5 and E16.5. This analysis included both the parietal and frontal calvaria bones, which have distinct embryonic tissue origins, and proliferative and osteogenic potential (Jiang et al., 2002; Xu et al., 2007; Quarto et al., 2010). In addition, sections were examined for alkaline phosphatase (ALP) activity, which is highly expressed in early osteoblast progenitors, and stained with Alizarin Red, which binds mineralised matrix.

These analyses revealed that Runx2, osterix, osteopontin and Bglap are expressed appropriately within the developing bones in *Dchs1*^{-/-} and *Fat4*^{-/-} mutants (Fig. 4C; Runx2 and osterix immunostaining: E15.5, wild type *n*=7, *Fat4*^{-/-} *n*=4, *Dchs1*^{-/-} *n*=3; E16.5, wild type *n*=7, *Fat4*^{-/-} *n*=4, *Dchs1*^{-/-} *n*=3; Bglap *in situ* hybridisation: E15.5/16.5, wild type *n*=8, *Fat4*^{-/-} *n*=4; *Dchs1*^{-/-} *n*=4; osteopontin *in situ* hybridisation: E15.5/16.5 wild type *n*=10, *Fat4*^{-/-} *n*=5, *Dchs1*^{-/-} *n*=5). ALP activity and mineralisation levels also appeared to be comparable: the latter is consistent with the μ -CT density measurements at P0 (Fig. 4B;

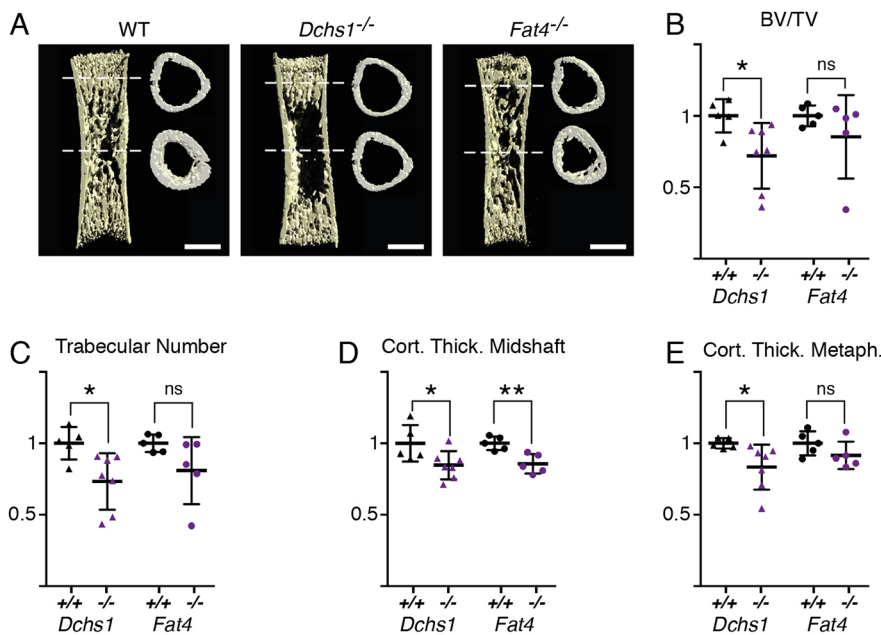


Fig. 2. *Dchs1* and *Fat4* are also required for appendicular skeletal development. (A) μ -CT scans of wild-type (WT; *n*=10), *Dchs1*^{-/-} (*n*=7) and *Fat4*^{-/-} (*n*=5) P0 pups showing sagittal views of the femur together with transverse cross-sections of the cortical bone at the levels indicated by the dashed lines. In some CT images, background 'noise/dots' may have been removed for clarity. (B-E) Quantification of the relative BV/TV (B), trabeculae number (C), cortical thickness at the midshaft (D) and metaphyses (E) where the average measurement of the control group was standardised to 1. Unpaired two-tailed Student's *t*-test: **P*<0.05; ***P*<0.01. ns, not significant. Error bars represent s.e.m. Scale bars: 0.5 mm.

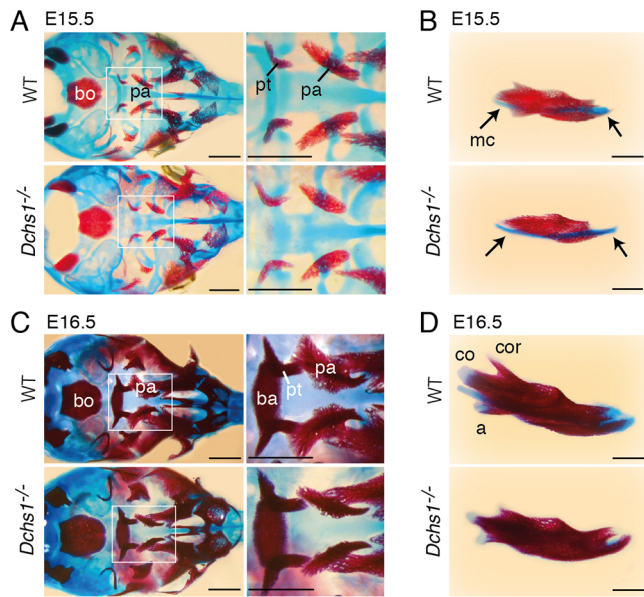


Fig. 3. Development of the cranial bones in *Dchs1* mutants. (A-D) Alizarin Red and Alcian Blue staining of E15.5 and E16.5 wild-type and *Dchs1*^{-/-} embryos; bone and cartilage are stained red and blue, respectively. (A,C) Cranial views of the cranial base and upper jaw at E15.5 ($n=2$) and E16.5 ($n=3$), respectively (the cranial vault has been removed); the right-hand side image is an enlarged image of the boxed area showing the palatine, basisphenoid and pterygoid bones. (B,D) Sagittal views of the mandible and Meckel's cartilage within the lower jaw at E15.5 and E16.5, respectively; Meckel's cartilage is indicated by arrows in B. a, angular process; ba, basisphenoid; bo, basioccipital; co, condylar process; cor, coronoid process; mc, Meckel's cartilage; pa, palatine; pt, pterygoid bones. Scale bars: 100 μ m.

Fig. S1C; ALP activity: E15.5, wild type $n=9$, *Fat4*^{-/-} $n=4$, *Dchs1*^{-/-} $n=4$; E16.5 wild type $n=10$; *Fat4*^{-/-} $n=5$, *Dchs1*^{-/-} $n=5$; mineralisation: E15.5, wild type $n=7$, *Fat4*^{-/-} $n=3$, *Dchs1*^{-/-} $n=4$; E16.5, wild type $n=7$, *Fat4*^{-/-} $n=5$, *Dchs1*^{-/-} $n=4$). However, there was a clear expansion in the numbers of Runx2^{+ve}osterix^{-ve} cells, the osteogenic progenitors, in both the palatine and calvaria bones (Fig. 4C). This expansion is also apparent by comparing the domains of ALP activity (Fig. 4B). Quantification of the number of Runx2^{+ve}osterix^{-ve} cells within the Runx2^{+ve} osteoprogenitor populations revealed that there was indeed a significant increase in the percentage of the Runx2^{+ve}osterix^{-ve} progenitors (Fig. 4D and data not shown; E15.5, *Fat4*^{+/+} $n=3$, *Fat4*^{-/-} $n=3$; palatine, $P<0.05$; frontal, $P<0.05$; E16.5, *Fat4*^{+/+} $n=3$, *Fat4*^{-/-} $n=3$; palatine, $P<0.01$; frontal, $P<0.05$; parietal, $P<0.01$).

Dchs1 and Fat4 regulate osteoblast proliferation, survival and differentiation

To determine whether changes in cell proliferation and/or cell survival contribute to the expansion of the osteoblast precursors, cells in the S and M phase of the cell cycle were identified by injection of 5-ethynyl-2'-deoxyuridine (EdU) and phospho-histone 3 immunostaining, respectively. Cells undergoing apoptosis were identified by immunolabelling for activated caspase 3.

These analyses revealed that proliferation within the Runx2^{+ve} cell population is significantly increased between E15.5 and E18.5 (Fig. 5A,B; Fig. S2A,B; E15.5 and E16.5: *Fat4*^{-/-} and *Dchs1*^{-/-} palatine, $P<0.01$; frontal, $P<0.05$; E16.5: *Fat4*^{-/-} parietal, $P<0.05$; E18.5: *Fat4*^{-/-} and *Dchs1*^{-/-} palatine, $P<0.05$; frontal, $P<0.05$; $n=3$ wild type and 3 mutants for each genotype and stage analysed). This increase in proliferation included the Runx2^{+ve}osterix^{+ve}

populations (Fig. 5A,B; $P<0.05$; palatine and frontal bones analysed). There was also a significant increase in proliferation associated with the trabecular bone of the femur, an endochondral bone, in *Dchs1*^{-/-}, but not *Fat4*^{-/-}, mutants. This is consistent with the differential requirements of Dchs1 and Fat4 within the endochondral bones that were observed in the μ -CT analyses (Fig. 2; Dchs1 $P<0.05$ and data not shown). In contrast, no or very few cells undergoing apoptosis were identified in either wild-type or mutant embryos at E16.5 (data not shown; wild type $n=3$, mutant $n=3$) but a significant increase in apoptosis within the osteogenic progenitors was observed at E18.5 (Fig. S2; $n=3$ wild type and 3 mutants; *Dchs1*^{-/-} and *Fat4*^{-/-} palatine, $P<0.01$; frontal, $P<0.05$).

This increased proliferation and expansion of the cell numbers in the osteogenic progenitor pool is inconsistent with the underdevelopment of the bones, indicating that it may be coupled with delayed differentiation. Alternatively, Dchs1-Fat4 may also be required within the terminally differentiating osteoblasts, where they are also expressed, and/or there may be increased osteoclast activity in the mutants. To investigate these possibilities, E16.5 embryos were labelled sequentially with calcein and Alizarin Red to identify the bone mineralisation front and osteoclast activity was analysed by tartrate-resistant acid phosphatase (TRAP) staining. In *Dchs1*^{-/-} embryos, the domain of calcein labelling was significantly smaller in the frontal and parietal bones compared with wild-type littermates (Fig. 5C; Fig. S5; $n=3$ each for *Dchs1*^{+/+} and *Dchs1*^{-/-}, $P<0.001$). In contrast, no observable differences in TRAP staining were identified ($n=3$; *Fat4*^{-/-} data not shown). These data suggest that the deficiency in bone architecture in Dchs1-Fat4 mutants is coupled with delayed osteoblast differentiation.

To determine whether Fat4 and Dchs1 are required within the terminally differentiated osteoblasts, Fat4 and Dchs1 expression was deleted using the osteocalcin (Bglap)-Cre line (OC-Cre). Cranial development was compared between the controls, OC-Cre^{Cre/+}; *Fat4*^{+/+} and OC-Cre^{Cre/+}; *Dchs1*^{fl/+}, and the OC-Cre^{Cre/+}; *Fat4*^{-/-} or OC-Cre^{Cre/+}; *Dchs1*^{-/-} mutants. In OC-Cre^{Cre/+}; *Fat4*^{-/-} pups, no significant differences in the development of the skull or facial bones were detected compared with the controls (Fig. S3; Table S5; OC-Cre^{Cre/+}; *Fat4*^{+/+} $n=3$, OC-Cre^{Cre/+}; *Fat4*^{-/-} $n=5$). In contrast, a minor decrease in bone volume was observed in the OC-Cre^{Cre/+}; *Dchs1*^{fl/-} mice compared with the controls (Fig. S3; Table S5; OC-Cre^{Cre/+}; *Dchs1*^{fl/+} $n=4$, OC-Cre^{Cre/+}; *Dchs1*^{fl/-} $n=5$; whole skull: $P<0.05$; frontal: $P<0.01$; parietal: $P<0.05$; palatine: $P<0.05$). The decrease in the size of the bones was, however, clearly less than that observed in *Dchs1* mutants (Fig. 1), indicating that the major roles of Dchs1 occur within the osteoprogenitors.

Dchs1- Fat4 signalling regulates Yap and Taz activity

In the developing cerebral cortex and heart, loss of Fat4 signalling is linked to increased Yap-dependent proliferation (Cappello et al., 2013; Ragni et al., 2017). To determine whether similar processes occur in bone, primary osteoblasts from *Fat4*^{+/+} and *Fat4*^{-/-} mutant P0 calvaria were transfected with either the Yap/Taz-Tea luciferase reporter construct, which measures Tead binding activity, or the control reporter containing mutated Tead-binding sites. These primary cultures comprise more than 97% Runx2^{+ve} cells on day 1 of culture (Fig. 6A) and express Bglap, indicative of terminal osteoblast differentiation, at later time points (Fig. 6A,B). In *Fat4*^{-/-} mutant cultures, however, there was a significant increase in the number of EdU-labelled cells (Fig. 6E; $P<0.001$) and an associated decrease in the percentage of Bglap-expressing cells at day 3 of culture (Fig. 6A,B; *Fat4*^{+/+} $n=3$, *Fat4*^{-/-} $n=3$, $P<0.001$). Thus, the

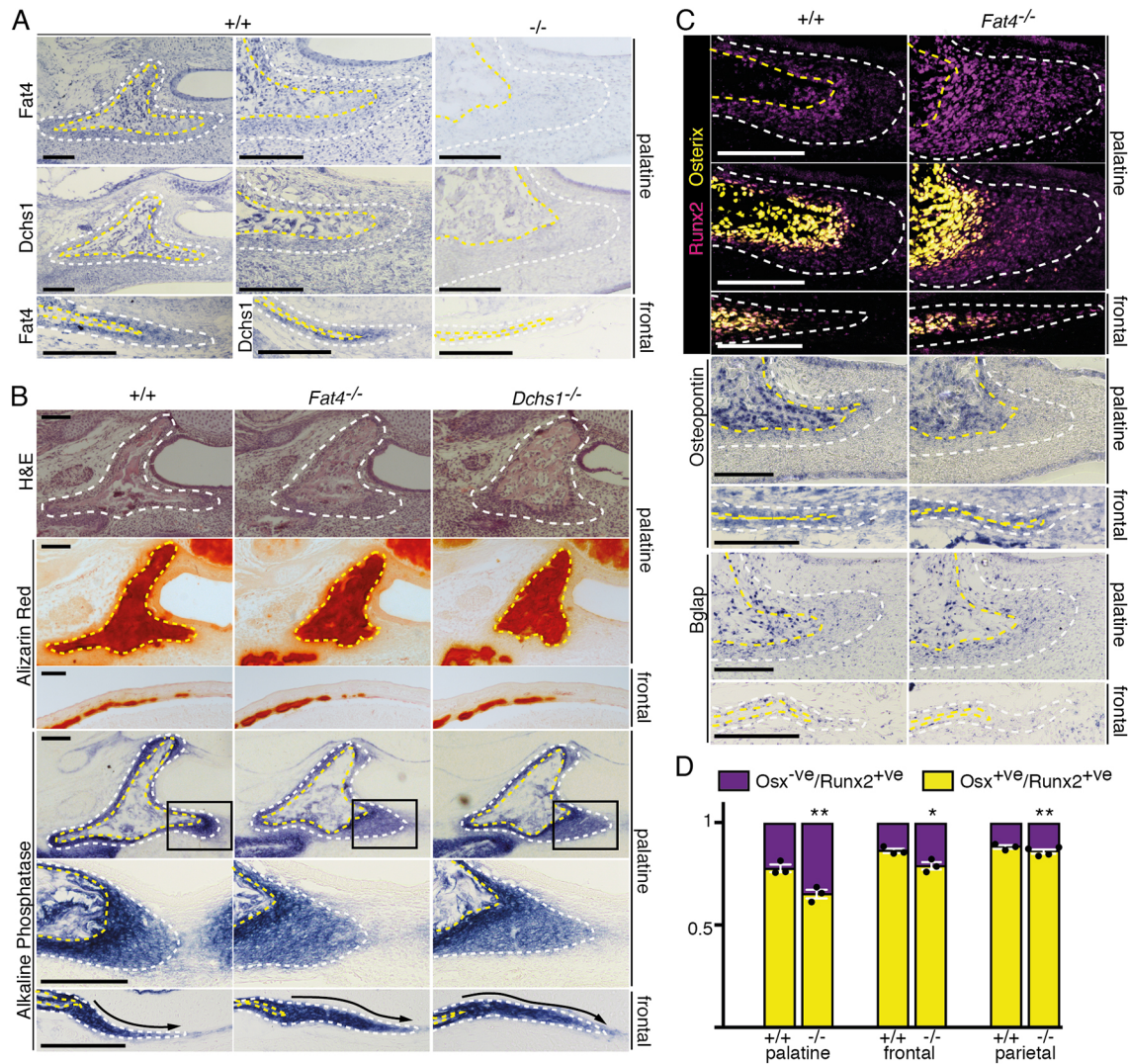


Fig. 4. Dchs1 and Fat4 regulate the number of osteoblast progenitors. (A) *In situ* hybridisation of *Fat4* and *Dchs1* expression in an E16.5 palatine (upper two rows) and frontal bone (lower row). Control *in situ* hybridisation on *Fat4* and *Dchs1* mutant tissue are shown on the right-hand side. (B) Frontal sections through the whole palatine and osteogenic front of the frontal bone showing Hematoxylin & Eosin (H&E) staining, mineralisation by Alizarin Red staining and alkaline phosphatase activity. For the ALP assay, a high-power view through the osteogenic fronts is shown for the palatine (boxed region of above lower power image). The length of the osteogenic fronts within the frontal bone is indicated by the arrows. (C) The osteogenic fronts of palatine and frontal bones in wild type and *Fat4*^{-/-} mutants showing Runx2 (magenta) and osterix (yellow) immunostaining and *in situ* hybridisation of osteopontin and *Eglap* where the blue staining indicates RNA expression. In A-C, the bones are outlined in white and the mineralised areas of the bone are outlined in yellow; the osteogenic progenitors are located between these lines. Number of biological replicates for each analyses stated in main text. (D) Quantification of the percentage of Osx^{-ve} (purple) and Osx^{+ve} (yellow) cell populations within the total Runx2 population of E16.5 palatine, frontal and parietal bones of *Fat4*^{+/+} (*n*=3 biological replicates) and *Fat4*^{-/-} (*n*=3) mutants. Unpaired two-tailed Student's *t*-test: **P*<0.05; ***P*<0.01. Error bars represent s.e.m.

in vitro cultures mimic *in vivo* osteogenesis. Using these cultures we found that the activity of the Yap/Taz-Tead, but not the control, luciferase reporter was significantly increased in *Fat4*^{-/-} osteoblasts (Fig. 6C; *Fat4*^{+/+} *n*=3; *Fat4*^{-/-} *n*=9, *P*<0.005). Similarly, activity of the Yap/Taz-Tead reporter was increased in *Dchs1*^{-/-} primary osteoblasts relative to either wild type or *Dchs1*^{+/+} controls (wild type *n*=6, *Dchs1*^{-/-} *n*=6, *P*<0.05; data not shown).

To help rule out the possibility that small differences in the starting cell population may contribute to the increased Yap/Taz-Tead signalling observed, we also assessed the effect of either *Fat4* or *Dchs1* knockdown in the osteogenic cell line MC3T3-E1. Again, we found that disruption of *Fat4*-*Dchs1* signalling led to increased Yap/Taz-Tead reporter activity (Fig. 6C; *n*=3; *Fat4* shRNA, *P*<0.01; *Dchs1* shRNA, *P*<0.05). We also confirmed that the 'Yap/Taz'

targets *Ctgf* (*Ccn2*), *Cyr61* (*Ccn1*) and *Ankrd1* were increased by qPCR of *Fat4* shRNA-treated MC3T3-E1 cells (*n*=3, *P*<0.005). Finally, we confirmed that gain of function of *Fat4* is sufficient to decrease Yap/Taz-Tead reporter activity in both primary cultures from wild-type and *Fat4*^{-/-} mice and in the MC3T3-E1 cell line (Fig. 6D; *Fat4*^{+/+} *n*=3, *P*<0.05; *Fat4*^{-/-} *n*=3, *P*<0.001; *Fat4* overexpression in MC3T3-E1 cells: control *n*=5, *Fat4* full length *n*=4, *P*<0.05). Collectively, the data indicate that *Dchs1*-*Fat4* signalling directly regulates Yap/Taz-Tead activity in osteoblasts.

Yap is the key regulator of Tead activity and proliferation within developing osteoblasts

To determine whether the increased Yap/Taz-Tead luciferase reporter activity in mutant cells is due to increased Yap and/or

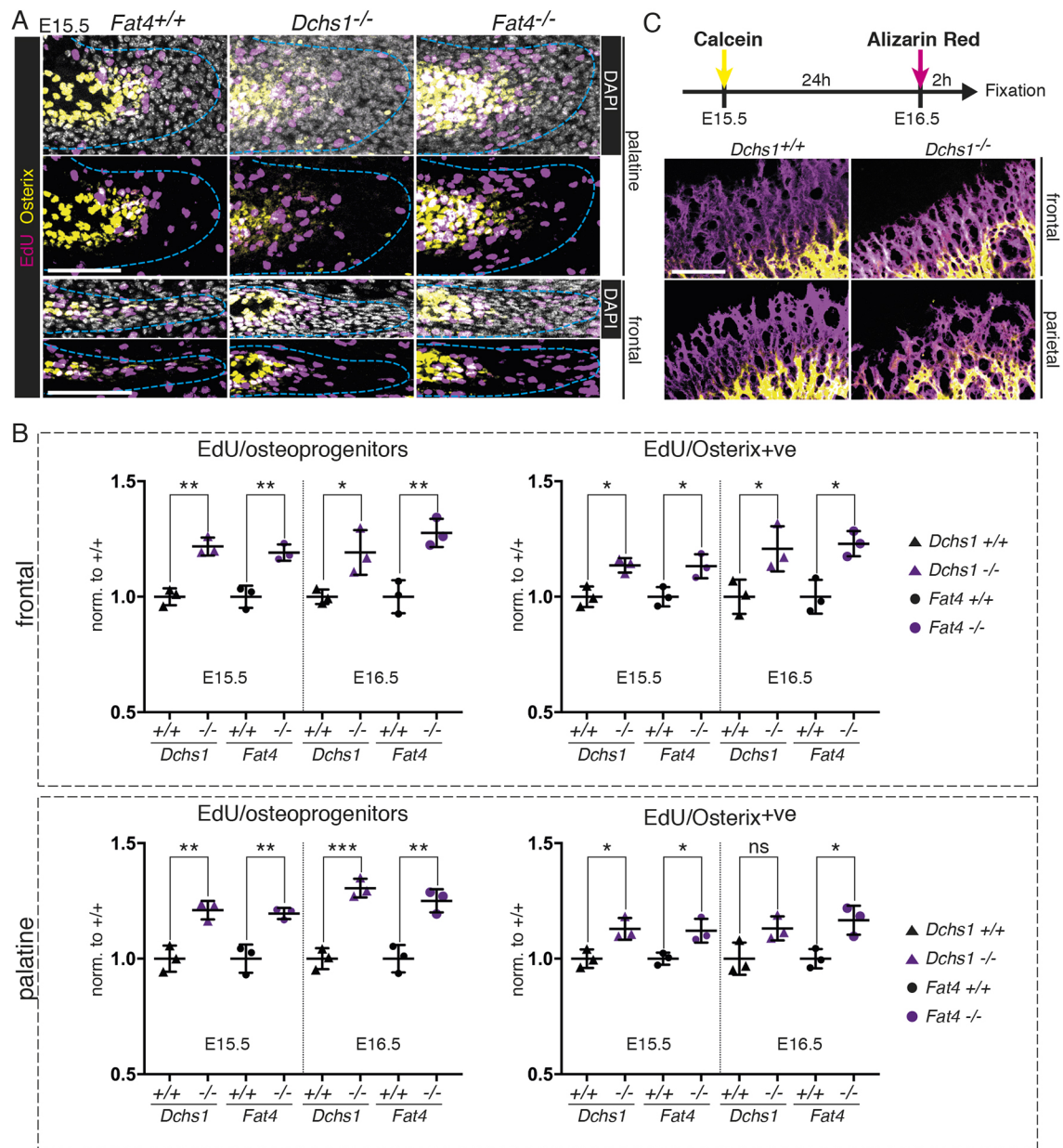


Fig. 5. *Dchs1*-*Fat4* regulation of osteoblast proliferation and differentiation. (A) Immunostaining of osteogenic fronts of palatine and frontal bones in E15.5 wild-type and *Fat4*^{-/-} embryos showing osterix expression (yellow) and EdU labelling of proliferating cells (magenta). DAPI staining (grey) is also shown. The boundary of the osteogenic front was identified by Runx2 staining (not shown) and is indicated by the dashed blue line. (B) Quantification of the number of proliferating cells (EdU labelled) within the Runx2⁺ osteoprogenitors (i.e. both the Runx2⁺osterix⁻ and Runx2⁺osterix⁺ cells) and within Runx2⁺osterix⁺ osteoprogenitors in the frontal and palatine bones. (C) Sequential calcein (yellow) and Alizarin Red (magenta) labelling of E16.5 osteogenic fronts in wild-type and *Dchs1*^{-/-} frontal and parietal bones ($n=3$ for each genotype). For B, within each control group the average measurement was standardised to 1. $n=3$ biological replicates for each genotype and each analysis. Unpaired two-tailed Student's *t*-test: * $P<0.05$; ** $P<0.01$; *** $P<0.005$. ns, not significant. Error bars represent s.e.m. Scale bars: 100 μ m.

Taz activity, *Yap* and *Taz* expression was knocked down in *Fat4*^{-/-} cells and the effect on the activity of the *Yap/Taz*-Tead luciferase reporter was measured. Both *Yap* and *Taz* shRNA knockdown significantly, and specifically, reduced *Yap* and *Taz* mRNA expression, respectively (Fig. 6F); however, only knockdown of *Yap* significantly reduced the activity of the 'Yap/Taz-Tead' luciferase reporter in wild-type and *Fat4*^{-/-} osteoblasts (Fig. 6E; $P<0.01$). In contrast, knockdown of *Taz* had no significant effect (Fig. 6E). Thus, *Yap* and *Taz* have distinct effects on the *Yap/Taz*-Tead reporter within the osteoblasts.

During the above studies we also observed that *Taz* mRNA expression is decreased in *Fat4*^{-/-} osteoblasts (Fig. 6F) and confirmed this regulation in MC3T3-E1 cells following knockdown of *Fat4* (Fig. 6F). Furthermore, our analysis of the *Taz*^{+/+} and *Taz*^{-/-} skeletal phenotype versus wild-type counterparts had revealed that a 50% reduction in *Taz* expression results in under-development of the cranial bones (Fig. S4A,B; Table S7). This raised the possibility that a decrease in the levels of *Taz* protein in *Fat4*^{-/-} osteoblasts may contribute to the mutant phenotype.

To examine this possibility, we carried out immunolocalisation analysis of *Taz* expression within the developing bones of wild type

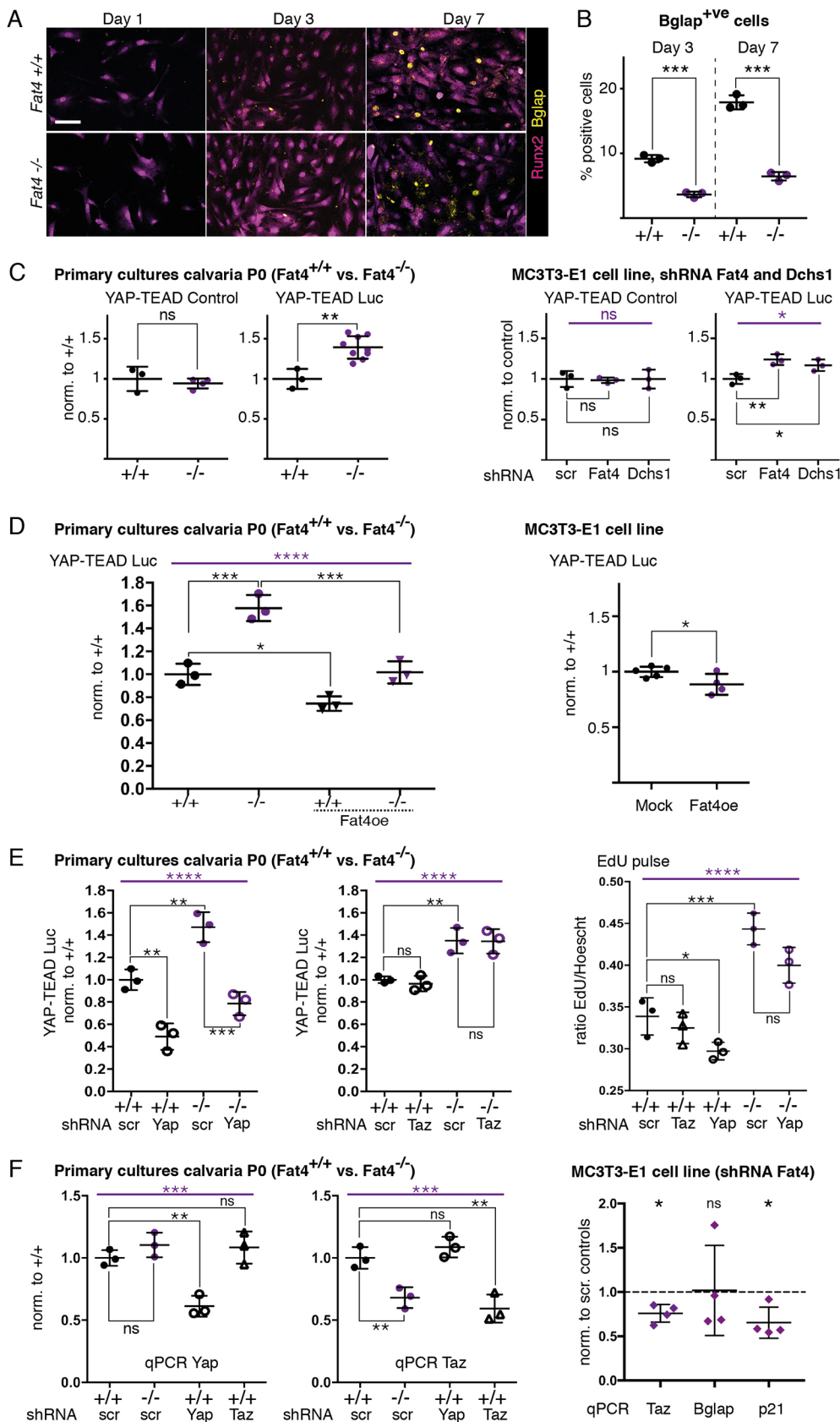


Fig. 6. *Dchs1* and *Fat4* regulate Yap activity. (A) Cultures of primary calvaria osteoblast cells from wild type ($n=3$ biological replicates) and *Fat4*^{-/-} ($n=3$) P0 mutants immunostained for Bglap (yellow), and co-stained for Runx2 (magenta). (B) Quantification of the percentage of Bglap⁺ cells at days 3 and 7 of culture. (C) Analysis of Yap/Taz-Teard reporter activity, and its control reporter, in primary *Fat4*^{+/+} and *Fat4*^{-/-} calvaria osteoblast cells, and in the MC3T3 cell line in which *Dchs1* and *Fat4* expression has been knocked down with shRNA constructs. (D) Analysis of Yap/Taz-Teard reporter activity in primary *Fat4*^{+/+} and *Fat4*^{-/-} calvaria osteoblast cells, and in the MC3T3 cell line following transfection of a vector encoding full-length *Fat4*. (E) Alteration in Yap/Taz-Teard reporter activity and proliferation in *Fat4*^{+/+} and *Fat4*^{-/-} calvaria osteoblasts following knockdown of either Yap or Taz. (F) qPCR analyses. Left and centre: Relative levels of *Yap* and *Taz* mRNA in *Fat4*^{-/-} osteoblasts compared with wild-type expression levels and validation of effective and specific knockdown of Yap and Taz using the shRNA constructs. Right: relative mRNA levels of *Taz*, *Bglap* and *p21* in MC3T3 cells transfected with shRNA for *Fat4*, compared with normalised levels (to 1) in control cells transfected with scrambled shRNA. For C-F, data points indicate each independent biological experiment i.e. $n \geq 3$, each with 2-3 technical replicates. Within each control group the average measurement was standardised to 100% (1 on graphs). Statistical analyses: unpaired two-tailed Student's *t*-tests for two group comparisons in B,C (left), and D (right), (significance shown in black); for three or more group comparisons, ordinary one-way ANOVA tests (significance shown in purple) were applied in C (right), D (left), E,F (left), followed by post-hoc analyses for multiple comparisons (significance shown in black) using Dunnett's tests in C (right), and F (left) and Tukey's tests in D (left), and E; in F, one sample *t*-test with a theoretical mean of 1 (relative mRNA expression value in control cells) for each set of qPCR data used. Significance: * $P < 0.05$, ** $P < 0.01$, *** $P < 0.001$, **** $P < 0.0001$. ns, not significant. Error bars represent s.e.m. Scale bar: 50 μ m. scr, scrambled shRNA plasmid.

and *Dchs1*^{-/-} mutants. We found that *Taz* expression is highest within the osteoblasts (Runx2⁺ Osterix⁺) adjacent to the mineralisation front and could not identify any obvious

differences in either the level or domain (nuclear/cytoplasmic) of *Taz* expression in *Dchs1*^{-/-} mutants (Fig. 7B). We also quantitatively determined the total levels of *Taz* protein in

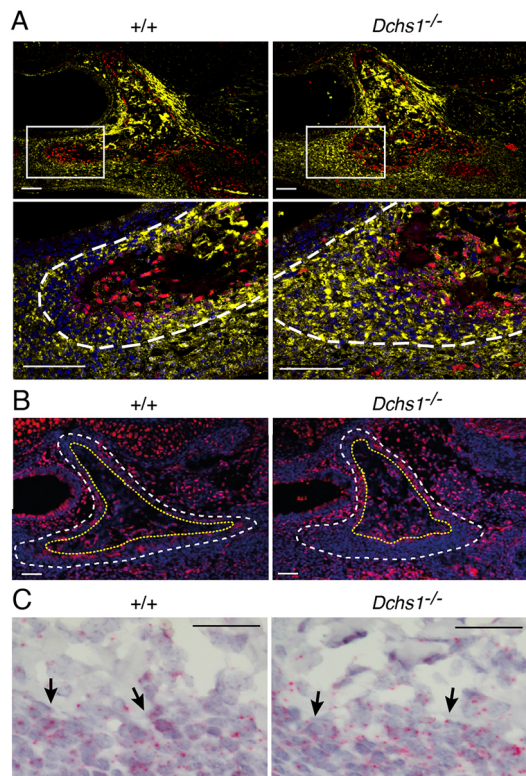


Fig. 7. Yap and Taz are differentially expressed within the developing bone. (A,B) Immunolocalisation and RNAScope analyses showing the expression of (A) Yap (yellow) and Osterix (red), (B) Taz (red) proteins and (C) *Taz* mRNA (red) in a palatine bone from wild-type and *Dchs1*^{-/-} E16.5 embryos. In A the boxed region is shown at higher magnification in the image below where the white lines indicate the bone boundary; the osteogenic progenitors are located just inside the white lines; the nuclei are stained with DAPI. In B, the borders of the bone and the mineralised region of the bones are demarcated by the white dashed and yellow dotted lines, respectively; the osteogenic progenitors are located between the two lines. Nuclei are stained with DAPI (blue). In C, the boundary between the osteocytes (upper part of image) and osteogenic progenitors (lower part of image) is demarcated by arrows; the red punctate staining indicates *Taz* mRNA. *n*=3 biological replicates for each genotype in each analysis. Scale bars: 100 μ m (A,B); 50 μ m (C).

MC3T3-E1 cells following knockdown of *Fat4* and *Dchs1*. However again, no detectable differences were observed (Fig. S6). Finally, given that we had found a decrease in *Taz* mRNA expression in *Fat4*^{-/-} osteoblasts *in vitro* we carried out RNAScope analyses to examine whether there are potential changes in either the domains or levels of *Taz* mRNA expression *in vivo*. This analysis did not identify any obvious changes (Fig. 7C and data not shown) but did reveal that *Taz* mRNA is expressed throughout the progenitor population, in contrast to the more restricted domain of Taz protein expression (Fig. 7B). We also determined the expression of Yap and found that Yap expression is highest in the very early *Runx2*^{+ve}*Osterix*^{-ve} osteoprogenitors, in contrast to the more restricted domain of Taz protein expression (Fig. 7B). In *Dchs1*^{-/-} mutants, the domain of Yap expression was expanded, consistent with the expansion of the progenitor domain (Fig. 7A).

The above analyses revealed differential expression of Yap and Taz: Yap is highest in a subpopulation of the *Runx2*^{+ve}*Osterix*^{-ve} progenitors whereas Taz is highest in *Runx2*^{+ve}*Osterix*^{+ve} cells. Both of these cell populations are proliferative. To analyse whether either Yap or Taz regulate proliferation, wild-type calvarial cells were

transfected with a shRNA-Yap or shRNA-Taz vector and cells in S phase were identified by a pulse of EdU. We found that cell proliferation was significantly decreased by Yap, but not by Taz, knockdown in wild-type osteoblasts (Fig. 6E; *P*<0.05). We then determined whether the increased Yap activity in *Fat4*^{-/-} osteoblasts is responsible for the increased cell proliferation that was observed. We found, however, that knockdown of Yap could reduce but not rescue the increased proliferation in *Fat4*^{-/-} osteoblasts (Fig. 6E).

Dchs1-Fat4 regulation of Runx2 activity

In MC3T3 and Ros17/2.8 cell lines, Yap gain of function has been shown to decrease activity of the *Runx2*-TGF β R1 reporter, have no significant effect on the activity of the generic *Runx2* promoter 6XOSE and enhance *Runx2* inhibition of the *Runx2*-*p21* promoter (Zaidi et al., 2004). To first investigate whether the function of the generic *Runx2* (6XOSE, containing part of the *Bglap* promoter), *Runx2*-*p21*, *Runx2*-TGF β R1 luciferase reporters was assessed in wild-type, *Fat4*^{-/-} and *Dchs1*^{-/-} mutant primary calvaria osteoblasts and the MC3T3-E1 cell line following knockdown of *Fat4* or *Dchs1*. We found that the activity of both the *Runx2*-*p21* and generic *Runx2* reporters was significantly decreased in *Fat4*^{-/-} and *Dchs1*^{-/-} primary cells (Fig. 8A and data not shown; *Fat4*^{+/+} *n*=3, *Fat4*^{-/-} *n*=6; *p21*, *P*<0.05; 6XOSE, *P*<0.01) and in the MC3T3-E1 cell line following knockdown of either *Fat4* or *Dchs1* (Fig. 8A; control *n*=3, *Fat4* shRNA *n*=3; *p21* *P*<0.01; 6XOSE *P*<0.05; *Dchs1* shRNA *n*=3, *p21* *P*<0.05, 6XOSE *P*<0.05). Conversely, the activity of the *Runx2*-TGF β R1 reporter is increased in mutant osteoblasts and in the MC3T3-E1 cell line following knockdown of *Fat4* (Fig. 8A; *Fat4*^{+/+} *n*=3, *Fat4*^{-/-} *n*=3, *P*<0.05; MC3T3-E1 shRNA: control *n*=3, *Fat4* shRNA *n*=3, *P*<0.05). Therefore, *Dchs1*-*Fat4* signalling differentially regulates the distinct *Runx2* promoters. The decreased activity of the *Runx2*-*p21* promoter was also associated with decreased *p21* expression in MC3T3-E1 cells following knockdown of *Fat4* (Fig. 6F).

To determine whether increased Yap activity contributes to the altered regulation of *Runx2* promoter activity observed in *Fat4*^{-/-} osteoblasts, Yap expression was knocked down in *Fat4*^{-/-} osteoblasts and the effect on the activity of the three *Runx2* reporters was analysed. This revealed that knockdown of Yap significantly decreased *Runx2*-TGF β R1 reporter activity in both wild-type and *Fat4*^{-/-} cells but had no effect on the 6XOSE and *p21* promoters (Fig. 8B,C; *Runx2*-TGF β R1 *P*<0.05). Thus, increased Yap is at least partly responsible for the increased activity of *Runx2*-TGF β R1 reporter activity observed in *Fat4*^{-/-} cells.

Although we did not detect any alterations in the levels of Taz expression or Taz-Tead activity in the previous studies, the activity of Taz can be qualitatively altered by post-transcriptional mechanisms such as through distinct binding partners or phosphorylation. To investigate whether Taz activity is also regulated by *Dchs1*-*Fat4* signalling, Taz expression was knocked down in wild-type and *Fat4*^{-/-} osteoblasts and the activity of the three *Runx2* reporters was analysed. This revealed that Taz regulates the activity of the *p21* and 6XOSE reporters but does not control activity of the TGF β R1 reporter in wild-type osteoblasts (Fig. 8B). Specifically, knockdown of Taz decreases the activity of the generic *Runx2* and *Runx2*-*p21* promoters in wild-type osteoblasts (Fig. 8B). However, knockdown of Taz could not further decrease the activity of these two reporters in mutant osteoblasts, potentially indicating that the activity of Taz-*Runx2* complexes is decreased in *Fat4*^{-/-} osteoblasts (Fig. 8C).

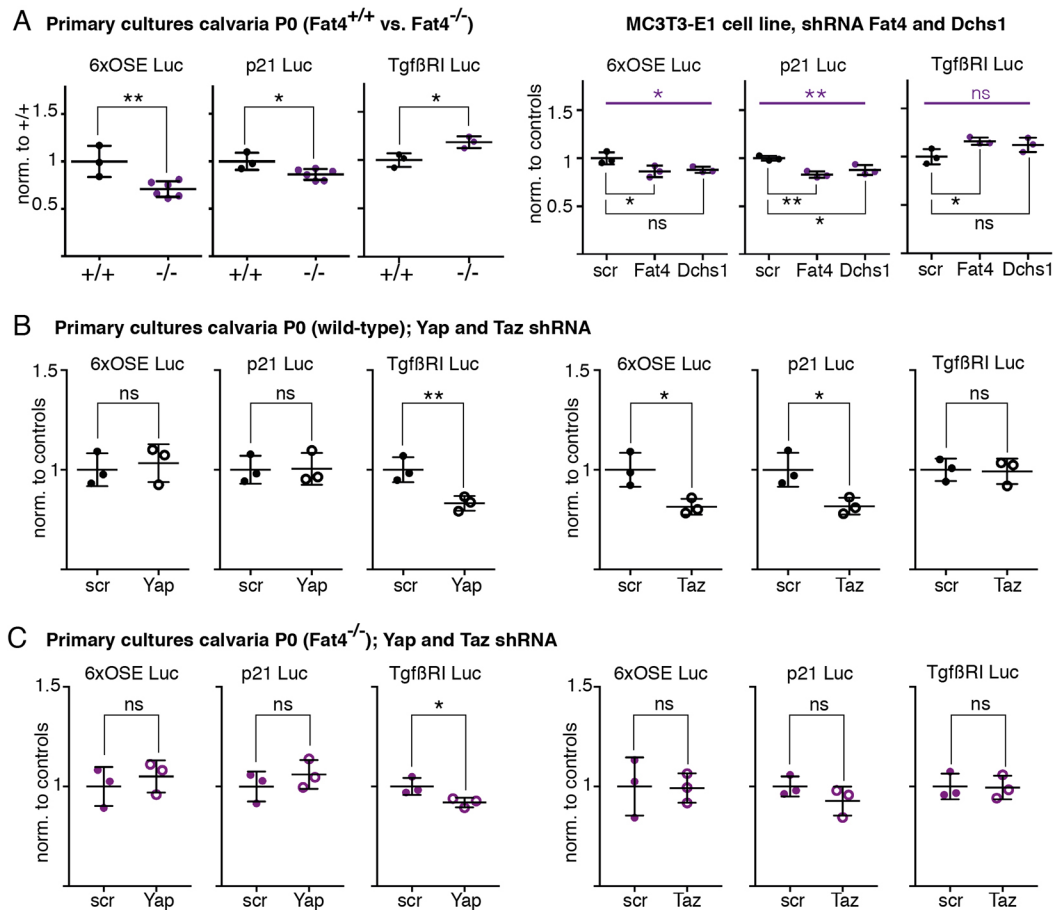


Fig. 8. *Dchs1* and *Fat4* regulate *Runx2* activity. (A) Activity of the *Runx2* reporters in primary *Fat4*^{+/+} and *Fat4*^{-/-} calvarial osteoblast cells, and the MC3T3 cell line in which *Fat4* expression has been knocked down with shRNA constructs. (B,C) The effect of knockdown of *Yap* and *Taz* expression on *Runx2* reporter activity in wild-type (B) and *Fat4*^{-/-} (C) osteoblasts. Data points indicate each independent biological experiment i.e. $n \geq 3$, each with 2-3 technical replicates. Within each control group, the average measurement was standardised to 1. scr, scrambled shRNA plasmid. (A, left-hand side, B, C) Unpaired two-tailed Student's *t*-tests. (A, right-hand side, B, C) One-way ANOVA (significance in purple) for multiple comparisons using post-hoc Dunnett's test (significance in black) * $P < 0.05$; ** $P < 0.01$. ns, not significant. Error bars represent s.e.m.

DISCUSSION

Here, we have shown that *Dchs1*-*Fat4* signalling regulates bone development by controlling proliferation, survival and differentiation within the osteogenic progenitors. Membrane bones of different tissue origins, neural crest (frontal, palatine), cranial mesoderm (parietal) and lateral plate mesoderm (bone collar of femur), are all affected in both *Dchs1* and *Fat4* mutants showing a global role of *Dchs1*-*Fat4* signalling in intramembranous ossification. In *Dchs1* mutants, the defects also encompassed many aspects of endochondral bone development. The abnormalities are consistent with the craniofacial phenotype of Van Maldergem patients and could also explain the increased susceptibility to fracture that has been reported in some patients (Mansour et al., 2012). Therefore, we have identified a new signalling pathway in bone development, together with mechanisms of action, which have relevance to our understanding of bone development and maintenance in humans.

At the cellular level, we identified that *Dchs1*-*Fat4* controls two key processes within the osteogenic progenitors, regulating both cell proliferation and progression along the differentiation pathway. We show that *Yap* activity is increased whereas *Taz*-*Runx2* activity is decreased. Both of these changes will contribute to the osteogenic defects. Increased *Yap* activity has also been shown to inhibit osteogenesis in the C3H10T1/2 cell line (Seo et al., 2013) and *Taz* is

essential for osteoblast differentiation (Cui et al., 2003; Hong et al., 2005). At the molecular level these effects are mediated, in part, by *Yap*/*Taz* regulation of *Runx2* activity. Increased expression of *Yap* targets, such as CTGF, which can increase osteoblast proliferation and inhibit differentiation, may also contribute to the phenotype (Mundy et al., 2014; Arnott et al., 2011). Additionally, at E18.5 there is also increased cell death within the osteogenic progenitors, which would contribute to the defects in bone development. This increased cell death may be secondary to altered cellular and morphological behaviours, as has been observed in the kidney (Mao et al., 2011, 2015), or paradoxically may be due to increased *Yap* signalling. In hepatocytes, overexpression of *Yap* has been shown to simultaneously promote both cell proliferation and cell death (Su et al., 2015) and as alterations in cell death were not found at E15.5 and E16.5, a similar mechanism may occur in E18.5 bones.

The increased proliferation within the osteogenic progenitors is analogous to the role of *Dchs1*-*Fat4* signalling in the cerebral cortex and heart (Cappello et al., 2013; Ragni et al., 2017) and in contrast to the decreased proliferation observed in the kidney and somites (Kuta et al., 2016; Mao et al., 2011). As in the heart and brain, loss of *Dchs1*-*Fat4* signalling also resulted in increased *Yap* activity. In the cerebral cortex and heart, knockdown of *Yap* activity through shRNA and genetic approaches was sufficient to fully rescue the

increased proliferation observed in *Fat4* mutants (Cappello et al., 2013; Ragni et al., 2017). In contrast, knockdown of Yap within the osteogenic progenitors, although decreasing proliferation, did not rescue the increased proliferation observed in *Fat4*^{-/-} cells. This may be due to a partial Yap knockdown and/or indicate that Dchs1-Fat4 regulate cell proliferation via Yap-independent mechanisms. However, Yap knockdown did result in a significant reduction in proliferation in wild-type osteoblasts. Therefore, at this point, although we cannot attribute the increased proliferation in *Fat4*^{-/-} osteoblasts to a Yap-dependent mechanism as has been observed in the heart and brain (Cappello et al., 2013; Ragni et al., 2017), we can definitively conclude that Yap is the major regulator of cell proliferation within wild-type osteoblasts and that, in contrast, Taz does not have a major proliferative role.

Our data additionally highlight the differential roles of Yap and Taz, which are often assumed to act redundantly. Within osteoblasts, Yap, but not Taz, has Tead-dependent activities. Teads are the main transcriptional binding partners for Yap and Taz and the ‘Hippo’ reporter measures Yap-Tead or Taz-Tead activity (Ehmer and Sage, 2016; Hansen et al., 2015). Our data indicate that Yap, but not Taz, has Tead-dependent activities within osteoblasts. Knockdown of Yap reduces ‘Hippo-Tead’ reporter activity in wild-type and *Fat4* mutant osteoblasts whereas Taz knockdown has minimal effect. Therefore, within developing osteoblasts Taz must mediate its functions via other transcriptional partners independently of Teads.

One candidate transcriptional partner is Runx2. Previous studies have shown that Taz and Yap have distinct effects on the activity of Runx2 (Cui et al., 2003; Hong et al., 2005; Zaidi et al., 2004). During this study, we have also extended previous analyses to show that Taz regulates the p21-Runx2 reporter. Yap can be inhibitory for osteogenesis (Seo et al., 2013) whereas Taz is required and sufficient to drive osteogenic differentiation (Hong et al., 2005; Yang et al., 2013). Therefore, within developing osteoblasts, it is essential that their expression and/or activity are uncoupled. We show that Yap regulates the Runx2-TGFβR1 but not the p21-Runx2 or generic Runx2 reporters. Specifically, we found that increased Yap in *Fat4*^{-/-} osteoblasts enhances Runx2-TGFβR1 reporter activity. These data differ from a previous study which indicated that Src-phosphorylated Yap (on tyrosine residues) inhibits Runx2 activation of the Runx2-TGFβR1 reporter and increases Runx2 suppression of the *p21* promoter (Zaidi et al., 2004). This difference may be due to the use of osteoblasts of different origin or that tyrosine-phosphorylation of Yap is altered by Dchs1-Fat4 signalling.

Our data also indicate that Taz-Runx2 transcriptional activity is decreased in *Dchs1*^{-/-} and *Fat4*^{-/-} osteoblasts. First, the activity of the Runx2-p21 and generic Runx2 6XOSE reporters, which are regulated by Taz in wild-type cells, is decreased following loss or knockdown of Dchs1-Fat4 signalling. Second, knockdown of Taz in *Fat4*^{-/-} mutant cells did not decrease reporter activity further. As levels of total Taz are unchanged, how this occurs is currently unclear. Potential mechanisms include changes in Taz binding to its potential co-transcriptional partners, or by the differential recruitment of proteins to the Taz-Runx2 transcriptional complex and/or by influencing the intracellular localisation of Taz.

The differential roles of Yap and Taz reflect their distinct expression patterns. Yap is expressed in the early osteoblast progenitors whereas Taz expression is more restricted within a population of more-differentiated osteoblasts adjacent to the mineralisation front. Of note, Yap and Taz expression was predominantly cytoplasmic with very low levels of Yap within

the nuclei and the immunolocalisation studies revealed no striking changes in Yap and Taz intracellular localisation in mutant osteoblasts. However, this does not indicate that Yap and Taz are inactive as Yap activity was clearly detected, and shown to be altered in mutant osteoblasts, by the more sensitive luciferase reporter assays and qPCR analysis of Yap/Taz targets, *Ctgf*, *Cyr61* and *Ankrd1*, with the potential caveat that these genes are also regulated by other signalling pathways. This predominantly cytoplasmic localisation of Yap has also been observed in postnatal trabecular osteoblasts where Yap controls proliferation (Pan et al., 2018). Also, levels of Yap can determine distinct cellular outputs, e.g. osteoblast versus adipocytes, and, therefore, a cytoplasmic bias in localisation does not indicate a lack of activity (Seo et al., 2013). The expression analyses also indicated that Taz protein and mRNA expression are uncoupled: *Taz* mRNA is found throughout the proliferative osteogenic progenitors in contrast to the more restricted protein expression domain. Therefore, within the osteoblast progenitors, Taz activity is controlled by post-translational mechanisms such as proteosomal degradation.

Although Fat4 signalling via Dchs2 has also been reported in the kidney (Bagherie-Lachidan et al., 2015), Fat4-Dchs1 typically act as a ligand-receptor pair. The craniofacial phenotypes are identical in the *Fat4* and *Dchs1* mutants, leading us to believe that here they also act as a ligand-receptor pair within the osteogenic progenitors during bone development. However, deletion of Dchs1, but not Fat4, within the differentiated osteoblasts [mediated via the osteocalcin (Bglap) Cre] resulted in a comparably minor craniofacial bone phenotype. Likewise, trabecular defects were also observed in the endochondrally derived femur bones of *Dchs1*, but not *Fat4*, mutants. This may indicate that Dchs1 acts through another Fat receptor such as Fat1, which can control Yap activity in fibroblasts (Martin et al., 2018). Alternatively there may be slight variations in the genetic background of the mutant mice. Within the Bglap-expressing cells it is also possible that Dchs1 in the more differentiated osteoblasts signals back to less-differentiated Fat4-expressing cells to drive osteogenic progression.

We have shown that Dchs1-Fat4 exert intrinsic control of bone development within osteoblast progenitors via regulation of cell proliferation, survival and Runx2 activity. Runx2 is the pivotal player during osteoblast development; it regulates osteoblast commitment, proliferation and ultimately progression along the osteogenic lineage to terminal differentiation (Komori, 2011; Long, 2011; Westendorf et al., 2002). Hence, levels of Runx2 expression and activity are finely tuned by the precise integration of a diverse array of signalling pathways, many of which impinge on Yap and Taz, which are also crucial regulators of osteogenesis. Thus, we have identified another osteogenic signalling pathway and shown at a cellular and molecular level how Dchs1-Fat4 signalling regulates osteoblast development. Crucially, the *Fat4* and *Dchs1* mutants phenocopy many aspects of Van Maldergem syndrome and thus our data provide a model and the foundations for understanding how this little-understood pathway regulates bone development and maintenance in humans.

MATERIALS AND METHODS

Mice

The mouse lines used were: *Dchs1*^{+/-} and *Dchs1*^{fl/fl} (Mao et al., 2011), *Fat4*^{+/-} and *Fat4*^{fl/fl} (Saburi et al., 2008), *Yap*^{+/-} (Mao et al., 2015) and *Taz*^{+/-} (*Wwtr1*) (Hossain et al., 2007), *Mesp1*-Cre (Saga et al., 1999), *Dermo1*-Cre (Yu et al., 2003), and osteocalcin-Cre (Bglap OC-Cre; Zhang et al., 2002). *Dchs1*, *Fat4* and all the Cre lines were maintained on a C57Bl/6J background whereas all fl/fl mice were maintained on a 129/SV

background. P0 and embryos for analysis were generated from the appropriate crosses. The day of the mouse plug was assigned E0.5.

All mouse procedures were reviewed and approved by the Institutional Animal Care and Use Committee (IACUC) at Rutgers University or the Use Committee of King's College (London, UK) under UK Home Office regulations; animal licence PPL 70/7328.

μ-CT analysis

Whole skulls and limbs from neonatal mice were μ-CT scanned (Skyscan1172 high-resolution μ-CT, Bruker, RVC, London). For all scans, calibration hydroxyapatite phantoms (Skyscan, Bruker) were used to facilitate conversion of the linear attenuation of a given voxel to mg HA/cm³. Skulls, individual bones within the skull (frontal, parietal, interparietal, palatine and mandible) and limbs (femur) were manually isolated, segmented, 3D reconstructed, and visualised using Bruker Software (NRecon, DATAVIEWER, CT-An and CT-Vox from Skyscan, Bruker) following manufacturer protocols and specifications. For the femur analysis, different volumes of interest (VOIs) were defined in the trabecular region, excluding the cortical shell, at mid-shaft (diaphysis, 50% of bone length) and distal (metaphysis, 33% of bone length) regions. For the femur, the following parameters were determined: bone volume fraction (BV/TV), cortical thickness and trabecular number. The size and bone mineral density were measured for the whole skull and the individual bones, applying the same thresholds for each litter to separate higher density bone from soft tissues and air. The selected VOIs were analysed using CT-An BatMan software (Skyscan, Kontich, Belgium) and 2D/3D morphometric parameters were recorded. In some CT scans, background 'noise/dots' between the bones in the CT scans has been removed for clarity.

Cell culture and reporter assays

Primary osteoblasts from neonatal mouse calvaria (frontal and parietal bones) were isolated and cultured as described by Taylor et al. (2014). Specifically, isolated individual calvaria were sequentially digested (at 37°C) for 10 min in 0.25% trypsin-EDTA (Sigma-Aldrich, T4049), 30 min in 0.2% collagenase (Sigma-Aldrich, C9891), with a final digestion in 0.2% collagenase for 1 h. The osteoblast cells were passaged for 2-4 days in growth media (Gibco, 10270-106) with 2 mM L-glutamine (AB/AM) and were then seeded at a density of 1.5×10^4 cells/well in 24-well plates and cultured in differentiation media (growth media with 10 mM β-glycerophosphate and 50 μg/ml ascorbic acid).

For the luciferase reporter assays, primary cells and the mouse osteoblast cell line MC3T3-E1 (ATCC CRL-2593, same media as primary cultures) were used. Cells were seeded at 1.5×10^4 cells/well in 24-well plates. On day 2-3 of culture, 250 ng of the reporter plasmid or shRNA vector together with 50 ng of *Renilla* plasmid were transfected into the primary osteoblasts or the MC3T3-E1 cell line using Lipofectamine LTX with Plus Reagent kit (Invitrogen, 15338-100) conforming to manufacturer instructions. The *Renilla* plasmid was used as an internal control to standardise the transfection efficiency. Luciferase reporter assays were carried out with Dual-Luciferase Reporter (DLR) Assay System (Promega, E1910) 48 h after lipofection; two or three technical replicates per experiment were measured and averaged. Each assay was repeated at least three times. Cell lines were tested for any mycoplasma contamination every 4 weeks.

Plasmids

Yap-Tead luciferase reporter, and its control reporter (Schlegelmilch et al., 2011), the Runx2 luciferase reporter plasmids (6XOSE, containing multimerised Runx2-binding sites), p21 or TGFβR1 (Zaidi et al., 2004), Dchs1, Fat4 or control siRNA (Cappello et al., 2013), Taz (Wwtr1, NM_133784, TRCN0000095951) and Yap (Yap1, NM_009534, TRCN0000238432) were obtained from MISSION shRNA library (Sigma-Aldrich).

qPCR

RNA was extracted from cultured cells using the RNeasy Micro Kit (Qiagen) and reverse transcribed to cDNAs with GoScript Kit (Promega). Quantitative PCR was carried out using Fast Start SYBR Green Master

(Roche) on a Bio-Rad CFX 384 (Bio-Rad) machine. Relative gene expression was quantified by the standard curve method using B2M as a control housekeeping gene. Primer sequences were: B2M forward CTGC-TACGTAACACAGTTCCACCC, B2M reverse CATGATGCTTGATCA-CATGTCTCG; Taz forward CCATCACTAATAATAGCTCAGATC, Taz reverse GTGATTACAGCCAGGTTAGAAAG; Yap forward CGGCAG-GCAATGCGGAATATCAAT, Yap reverse ACCATCCTGCTCCAGTG-TTGGTAA; p21 forward GCCTTAGCCCTCACTCTGTG, p21 reverse AGGGCCCTACCGTCCCTACTA; Bglap forward CCGGAGCAGTGT-GAGCTTA, Bglap reverse TAGATGCGTTTTGTAGGCGGTC; Ctgf, forward GACCCAATATGATGCGAGCC, Ctgf reverse CCCATCCCA-CAGGTCTTAGAAC; Cyr61 forward AGAGGCTTCTGTCTTTGGC, Cyr61 reverse CCAAGACGTGGTCTGAACGA; Ankrd forward TGCG-ATGAGTATAAACGGACG, Ankrd reverse GTGGATTCAAGCATA-TCTCGGAA.

RNAScope

Formalin-fixed paraffin-embedded samples were analysed with RNAScope 2.5 assay (Advanced Cell Diagnostic) using a RNAScope 2.5 HD-Red kit (Wang et al. 2012). Samples were cut at 5 μm thickness and processed according to manufacturer's recommendations. Freshly cut sections were incubated in a hybridisation oven for 1 h at 60°C and subsequently deparaffinised. The slides were treated with hydrogen peroxide solution for 10 min at room temperature. For E16.5 embryos, the standard pre-treatment recommendations were followed. Samples were boiled in target retrieval solution for 15 min keeping the temperature between 98 and 102°C. After 30 min incubation at 40°C with protease plus reagent, sections were hybridised with the following probes for 2 h at 40°C: WWTR1 (Taz), PPIB (positive control), and DapB (negative control), all from Advanced Cell Diagnostics. Sections were then incubated with the signal amplification solutions in the following order: amp1 for 30 min at 40°C, amp2 for 15 min at 40°C, amp3 for 30 min at 40°C, amp4 for 15 min at 40°C, amp5 for 30 min at room temperature, amp6 for 15 min at room temperature. Finally, slides were incubated with Fast Red solution for 10 min at room temperature to detect the signal. Samples were counterstained with Gill's Hematoxylin I and mounted using VectaMount mounting medium (Vector labs). The results were analysed with a standard brightfield microscope (Zeiss Axioskop with a Nikon DS-Fi2 camera) at 40× magnification.

Whole-mount and *in vivo* skeletal analysis

Alcian Blue and Alizarin Red staining of P0 pups, E15.5 and E16.5 heads was performed to analyse bone development. Bone deposition and resorption were also evaluated by intraperitoneal injections of calcein (Sigma-Aldrich, C0875; 2.5 mg/kg body weight) into pregnant females at E15.5 and Alizarin Complexone (Sigma-Aldrich, a3882; 7.5 mg/kg) at E16.5. The calvarias were collected 2 h after the Alizarin Complexone injection and fixed overnight in 4% paraformaldehyde (PFA) in PBS. They were washed in PBS and flat-mounted for imaging by confocal microscopy using a Leica SP5 confocal microscope.

Histological and immunolocalisation assays

Embryos were dissected in cold PBS (RNase free), fixed overnight in 4% PFA at 4°C and dehydrated through an increasing series of alcohols (50, 70, 80, 85, 90, 95% and absolute ethanol) and embedded in paraffin. Frontal sections (10-12 μm) were mounted and used for *in situ* hybridisation, immunostaining or chemical staining. One mutant embryo paired with one control littermate were processed together and mounted on the same slides. To determine alkaline phosphatase activity, sections were incubated in NMT buffer (100 mM Tris HCl pH 9.5, 50 mM MgCl₂, 100 mM NaCl) with 5-bromo-4-chloro-3-indolyl-phosphate (BCIP; 3.4 μl/ml; Roche, 11383221001) and 4-nitro blue tetrazolium (NBT; 4.5 μl/ml; Roche, 11383213001) for 12 min at room temperature in the dark. To determine levels of mineralisation, sections were stained in Alizarin Red solution (pH 4.2, 2% 3,4-dihydroxy-9,10-dioxo-2-anthracenesulfonic acid sodium salt, Sigma-Aldrich, A3757, in distilled H₂O) for 5-8 min. TRAP activity was determined on 10 μm PFA-fixed sections using a leucocyte acid phosphatase (Trap) kit (Sigma-Aldrich, 387A 1KT).

For immunostaining, de-waxed slides were treated in antigen retrieval buffer (10 mM citric acid pH 6.4) in a pressure cooker for 6.5 min. Sections were blocked in 2% bovine serum albumin, 5% goat serum, for 30 min at room temperature in a humid chamber and then counterstained with 1% Sudan Black B (Sigma-Aldrich, 199664) to reduce autofluorescence. For Runx2 immunostaining, a biotin amplification step using biotinylated goat anti-mouse IgG antibody (Vectashield, BA-9200) and Streptavidin 488 (Biolegend, 405235) was carried out. For Yap and Taz immunostaining, a PerkinElmer TSA Cyanine 3 System (NEL704A001KT) was used. Primary mouse osteoblast cells plated on glass coverslips were fixed in 4% PFA for 20 min, washed in PBS, blocked and immunostained. The following primary antibodies were used: Runx2 (Abcam, ab76956, 1:100), osterix (Abcam, ab22552, 1:1000), caspase 3 (Cell Signaling Technology, 9661S, 1:200), Bglap (Santa Cruz Biotechnology, sc-30045, 1:100), Yap (Santa Cruz Biotechnology, sc-101199; 1:1000), Taz (Atlas, HPA007415, 1:2000). The secondary antibodies were donkey anti-mouse 594 (Invitrogen, A21203, 1:500), donkey anti-rabbit 488 (Invitrogen, A21206, 1:500), donkey anti-rabbit 568 (Invitrogen, A10042, 1:500). Sections/cells were counterstained with DAPI.

In situ hybridisation

In situ hybridisation to tissue sections was carried out as described by Mao et al. (2011) using [50% formamide, 5× SSC, 50 µg/ml heparin (Sigma-Aldrich, H3393), 50 mg/ml total yeast RNA, 50 µg/ml SSDNA (Invitrogen, 15632-011) and 0.1% SDS] for prehybridisation at 65°C for 2 h. Sections were incubated overnight with the corresponding digoxigenin (DIG)-labelled antisense RNA probe in hybridisation buffer (pre-hybridisation buffer without total yeast RNA). Unbound probe was removed by washing at increasing stringency: 62°C (two 30 min washes in 50% formamide, 5× SSC, 1% SDS) and 60°C (two 30 min washes in 50% formamide, 2× SSC, 0.2% SDS). Slides were washed in MABT solution (maleic acid buffer containing 0.1% Tween 20) and blocked in 10% sheep serum for 1 h before incubating overnight at 4°C with anti-DIG antibody (1:2000 dilution). Unbound antibody was removed by six washes in PBST (PBS containing 0.1% Tween 20; 8 min, rocking) at room temperature. Bound probe was visualised by staining with NBT/BCIP at pH 9.5 in NMT buffer (see above). The following probes were used: Dchs1 (Mao et al., 2011), Fat4 (Mao et al., 2011), Bglap (Lana-Elola et al., 2007), osteopontin (Young et al., 1990).

Proliferation and cell counting analyses

To label cells in the S phase of the cell cycle pregnant females were injected intraperitoneally with EdU (200 mg/kg) at a gestation age of E15.5 and E16.5. Embryos were collected 4 h later and processed for immunolocalisation analyses. For primary cell cultures, cells were plated onto glass coverslips and pulsed with 20 µM EdU for 2 h. Cells were then washed in PBS and fixed in 4% PFA for 10 min. EdU-labelled cells were detected with Click-iT Plus EdU Alexa Fluor 594 Imaging Kit (Molecular Probes, C10639) following the manufacturer's protocol. Alternatively, cells undergoing mitosis were identified by immunostaining for phospho-histone H3 (Cell Signaling Technology, 9706L, 1:500).

Following immunostaining, cells from confocal images (20× objective) were manually counted using ImageJ software (Rasband, W.S., ImageJ, U. S. National Institutes of Health, Bethesda, Maryland, USA, <http://imagej.nih.gov/ij/>, 1997-2016) from at least six sections per embryo or at least five different microscopic fields within a primary culture.

Western blot analysis

Western blot analysis was carried out on total proteins extracted from cell cultures (MC3T3 E1) 48 h after transfection with either scrambled control (scr) or Dchs1 shRNA or Fat4 shRNA, using Passive Lysis 5X buffer (Promega, E194A), and on liver tissue from wild-type or *Taz*^{-/-} adult mice using RIPA lysis buffer (150 mM NaCl, 1% NP-40, 0.5% DOC, 0.1% SDS, 50 mM Tris pH 7.4), which included a protease and phosphatase inhibitor cocktail. Protein concentration was measured at 560 nm using a BCA protein assay kit (Novagen, 71258) according to manufacturer's recommendations. Lysates (10 µg) of prepared in Laemmli Buffer (Bio-Rad, 1610747) were boiled at 95°C for 5 min and then resolved by SDS-PAGE. Proteins were transferred onto PVDF membranes using a Trans-blot

Turbo transfer system (Bio-Rad) and blocked with 5% non-fat milk for 1 h at room temperature. Membranes were incubated overnight at 4°C with the primary antibodies anti-WWTR1 (1:1000, Atlas, HPA007415) and anti-cyclophilin B, the loading control (1:1000, R&D Systems, MAB5410), followed by incubation with the anti-mouse or anti-rabbit HRP-conjugated secondary antibodies (1:2000, Dako, P0448 and P0447). Proteins of interest were detected with an ECL substrate (Bio-Rad, 1705060) and imaged with Chemidoc Imaging system (Bio-Rad). Densitometric analysis was carried out using ImageJ software and the signal of the protein of interest was normalised to the loading control.

Statistical analysis

To compare and standardise the results, the average value for wild-type or controls was normalised to 1. The wild-type, heterozygote, mutant or control/experimental value were then standardised as a ratio of the average wild-type number. All stated numbers (*n*) are for different biological replicates (either *in vivo* or *in vitro*). For the cell culture experiments, at least three technical replicates were analysed and the average used. The significance of the data was determined using unpaired Student's *t*-test comparing control/experimental or wild type/mutant pairs. Each data pair was analysed individually. Within the graphs, the control bar combines the individual control values from each data set. Sample size, *n*=3-5. No samples or datasets were excluded from the analyses.

Acknowledgements

We thank Gerard Karsenty for the gift of the Runx2 antibody; Helen McNeill for the gift of Fat4 mouse mutants; David Ornitz for the Dermo1^{Cre} and Osteocalcin^{Cre} mouse lines; Drs Silvia Cappello and Magdalena Goetz for the Dchs1 and Fat4 shRNA constructs; Dr Fernando Camargo for the gift of the Yap/Taz reporter constructs and Dr G. Stein for the Runx2 reporter constructs. We also thank Mark Hopkinson (RVC) and Chris Healy (KCL) for carrying out the µ-CT scans, Dr Isabel Orriss (RVC) for guidance with primary cultures and Dr Gernot Walko for critically reading the manuscript.

Competing interests

The authors declare no competing or financial interests.

Author contributions

Conceptualization: S.A., A.A.P., K.D.I., P.F.-W.; Methodology: I.C.-E., T.H., S.Z., E.C., M.S., A.A.P., P.F.-W.; Formal analysis: I.C.-E., T.H., S.Z., E.C., A.A.-K., G.V.-O., P.F.-W.; Investigation: I.C.-E., T.H., S.Z., E.C., S.A., A.A.-K., Y.M., A.Y., G.V.-O., J.P., P.F.-W.; Resources: A.A.P., K.D.I., P.F.-W.; Writing - original draft: I.C.-E., P.F.-W.; Writing - review & editing: P.F.-W.; Supervision: A.A.P., K.D.I., P.F.-W.; Project administration: A.A.P., P.F.-W.; Funding acquisition: A.A.P., K.D.I., P.F.-W.

Funding

This research was funded by the Biotechnology and Biological Sciences Research Council (BB/K008668/1 to P.F.-W., A.A.P.); the Howard Hughes Medical Institute; a National Institutes of Health grant (R01 GM078620 to K.D.I.); and a Kings College London PhD Scholarship (S.Z., P.F.-W.). Deposited in PMC for release after 12 months.

Supplementary information

Supplementary information available online at <http://dev.biologists.org/lookup/doi/10.1242/dev.176776.supplemental>

References

- Arnott, J. A., Lambi, A. G., Mundy, C., Hendsi, H., Pixley, R. A., Owen, T. A., Safadi, F. F. and Popoff, S. N. (2011). The role of connective tissue growth factor (CTGF/CCN2) in skeletogenesis. *Crit. Rev. Eukaryot. Gene Expr.* **21**, 43-69. doi:10.1615/CritRevEukarGeneExpr.v21.i1.40
- Bagherie-Lachidan, M., Reginensi, A., Zaveri, H. P., Scott, D. A., Helmbacher, F. and McNeill, H. (2015). Stromal Fat4 acts non-autonomously with Dachsous1/2 to restrict the nephron progenitor pool. *Development* **142**, 2564-2573. doi:10.1242/dev.122648
- Cappello, S., Gray, M. J., Badouel, C., Lange, S., Einsiedler, M., Srour, M., Chitayat, D., Hamdan, F. F., Jenkins, Z. A., Morgan, T. et al. (2013). Mutations in genes encoding the cadherin receptor-ligand pair DCHS1 and FAT4 disrupt cerebral cortical development. *Nat. Genet.* **45**, 1300-1308. doi:10.1038/ng.2765
- Cui, C. B., Cooper, L. F., Yang, X., Karsenty, G. and Aukhil, I. (2003). Transcriptional coactivation of bone-specific transcription factor Cbfa1 by TAZ. *Mol. Cell. Biol.* **23**, 1004-1013. doi:10.1128/MCB.23.3.1004-1013.2003

- Das, A., Tanigawa, S., Karner, C. M., Xin, M., Lum, L., Chen, C., Olson, E. N., Perantoni, A. O. and Carroll, T. J. (2013). Stromal-epithelial crosstalk regulates kidney progenitor cell differentiation. *Nat. Cell Biol.* **15**, 1035-1044. doi:10.1038/ncb2828
- Dupont, S., Morsut, L., Aragona, M., Enzo, E., Giulitti, S., Cordenonsi, M., Zanconato, F., Le Digabel, J., Forcato, M., Bicciato, S. et al. (2011). Role of YAP/TAZ in mechanotransduction. *Nature* **474**, 179-183. doi:10.1038/nature10137
- Ehmer, U. and Sage, J. (2016). Control of proliferation and cancer growth by the hippo signaling pathway. *Mol. Cancer Res.* **14**, 127-140. doi:10.1158/1541-7786.MCR-15-0305
- Galea, G. L., Meakin, L. B., Savery, D., Taipaleenmaki, H., Delisser, P., Stein, G. S., Copp, A. J., van Wijnen, A. J., Lanyon, L. E. and Price, J. S. (2015). Planar cell polarity aligns osteoblast division in response to substrate strain. *J. Bone Miner. Res.* **30**, 423-435. doi:10.1002/jbmr.2377
- Hansen, C. G., Moroiishi, T. and Guan, K. L. (2015). YAP and TAZ: a nexus for Hippo signaling and beyond. *Trends Cell Biol.* **25**, 499-513. doi:10.1016/j.tcb.2015.05.002
- Hong, J. H., Hwang, E. S., McManus, M. T., Amsterdam, A., Tian, Y., Kalmukova, R., Mueller, E., Benjamin, T., Spiegelman, B. M., Sharp, P. A. et al. (2005). TAZ, a transcriptional modulator of mesenchymal stem cell differentiation. *Science* **309**, 1074-1078. doi:10.1126/science.1110955
- Hossain, Z., Ali, S. M., Ko, H. L., Xu, J., Ng, C. P., Guo, K., Qi, Z., Ponniah, S., Hong, W. and Hunziker, W. (2007). Glomerulocystic kidney disease in mice with a targeted inactivation of Wwtr1. *Proc. Natl. Acad. Sci. USA* **104**, 1631-1636. doi:10.1073/pnas.0605266104
- Irvine, K. D. and Harvey, K. F. (2015). Control of organ growth by patterning and hippo signaling in *Drosophila*. *Cold Spring Harb. Perspect Biol.* **7**, a019224. doi:10.1101/cshperspect.a019224
- Jiang, X., Iseki, S., Maxson, R. E., Suvoc, H. M. and Morriss-Kay, G. M. (2002). Tissue origins and interactions in the mammalian skull vault. *Dev. Biol.* **241**, 106-116. doi:10.1006/dbio.2001.0487
- Komori, T. (2011). Signaling networks in RUNX2-dependent bone development. *J. Cell. Biochem.* **112**, 750-755. doi:10.1002/jcb.22994
- Komori, T., Yagi, H., Nomura, S., Yamaguchi, A., Sasaki, K., Deguchi, K., Shimizu, Y., Bronson, R. T., Gao, Y. H., Inada, M. et al. (1997). Targeted disruption of *Cbfa1* results in a complete lack of bone formation owing to maturational arrest of osteoblasts. *Cell* **89**, 755-764. doi:10.1016/S0092-8674(00)80258-5
- Kuta, A., Mao, Y., Martin, T., Ferreira de Sousa, C., Whiting, D., Zakaria, S., Crespo-Enriquez, I., Evans, P., Balczerki, B., Mankoo, B. et al. (2016). Fat4-Dchs1 signalling controls cell proliferation in developing vertebrae. *Development* **143**, 2367-2375. doi:10.1242/dev.131037
- Lana-Elola, E., Rice, R., Grigoriadis, A. E. and Rice, D. P. (2007). Cell fate specification during calvarial bone and suture development. *Dev. Biol.* **311**, 335-346. doi:10.1016/j.ydbio.2007.08.028
- Long, F. (2011). Building strong bones: molecular regulation of the osteoblast lineage. *Nat. Rev. Mol. Cell Biol.* **13**, 27-38. doi:10.1038/nrm3254
- Mansour, S., Swinkels, M., Terhal, P. A., Wilson, L. C., Rich, P., Van Maldergem, L., Zwijnenburg, P. J. G., Hall, C. M., Robertson, S. P. and Newbury-Ecob, R. (2012). Van Maldergem syndrome: further characterisation and evidence for neuronal migration abnormalities and autosomal recessive inheritance. *Eur. J. Hum. Genet.* **20**, 1024-1031. doi:10.1038/ejhg.2012.57
- Mao, Y., Mulvaney, J., Zakaria, S., Yu, T., Morgan, K. M., Allen, S., Basson, M. A., Francis-West, P. and Irvine, K. D. (2011). Characterization of a Dchs1 mutant mouse reveals requirements for Dchs1-Fat4 signaling during mammalian development. *Development* **138**, 947-957. doi:10.1242/dev.057166
- Mao, Y., Francis-West, P. and Irvine, K. D. (2015). A Fat4-Dchs1 signal between stromal and cap mesenchyme cells influences nephrogenesis and ureteric bud branching. *Development* **142**, 2574-2585. doi:10.1242/dev.122630
- Mao, Y., Kuta, A., Crespo-Enriquez, I., Whiting, D., Martin, T., Mulvaney, J., Irvine, K. D. and Francis-West, P. (2016). Dchs1-Fat4 regulation of polarized cell behaviours during skeletal morphogenesis. *Nat. Commun.* **7**, 11469. doi:10.1038/ncomms11469
- Martin, D., Degese, M. S., Vitale-Cross, L., Iglesias-Bartolome, R., Valera, J. L. C., Wang, Z., Feng, X., Yeerna, H., Vadmal, V., Moroiishi, T. et al. (2018). Assembly and activation of the Hippo signalingome by FAT1 tumor suppressor. *Nat. Commun.* **9**, 2372. doi:10.1038/s41467-018-04590-1
- Matis, M. and Axelrod, J. D. (2013). Regulation of PCP by the fat signaling pathway. *Genes Dev.* **27**, 2207-2220. doi:10.1101/gad.228098.113
- Misra, J. R. and Irvine, K. D. (2018). The hippo signaling network and its biological functions. *Annu. Rev. Genet.* **52**, 65-87. doi:10.1146/annurev-genet-120417-031621
- Mundy, C., Gannon, M. and Popoff, S. N. (2014). Connective tissue growth factor (CTGF/CCN2) negatively regulates BMP-2 induced osteoblast differentiation and signaling. *J. Cell. Physiol.* **229**, 672-681. doi:10.1002/jcp.24491
- Neuhann, T. M., Muller, D., Hackmann, K., Holzinger, S., Schrock, E. and Di Donato, N. (2012). A further patient with van Maldergem syndrome. *Eur. J. Med. Genet.* **55**, 423-428. doi:10.1016/j.ejmg.2012.02.012
- Otto, F., Thornell, A. P., Crompton, T., Denzel, A., Gilmour, K. C., Rosewell, I. R., Stamp, G. W., Beddington, R. S., Mundlos, S., Olsen, B. R. et al. (1997). *Cbfa1*, a candidate gene for cleidocranial dysplasia syndrome, is essential for osteoblast differentiation and bone development. *Cell* **89**, 765-771. doi:10.1016/S0092-8674(00)80259-7
- Pan, J.-X., Xiong, L., Zhao, K., Zeng, P., Wang, B., Tang, F.-L., Sun, D., Guo, H. H., Yang, X., Cui, S. et al. (2018). YAP promotes osteogenesis and suppresses adipogenic differentiation by regulating beta-catenin signaling. *Bone Res.* **6**, 18. doi:10.1038/s41413-018-0018-7
- Quarto, N., Wan, D. C., Kwan, M. D., Panetta, N. J., Li, S. and Longaker, M. T. (2010). Origin matters: differences in embryonic tissue origin and Wnt signaling determine the osteogenic potential and healing capacity of frontal and parietal calvarial bones. *J. Bone Miner. Res.* **25**, 1680-1694. doi:10.1359/jbmr.091116
- Ragni, C. V., Diguët, N., Le Garrec, J.-F., Novotova, M., Resende, T. P., Pop, S., Charon, N., Guillemot, L., Kitasato, L., Badouel, C. et al. (2017). Amotl1 mediates sequestration of the Hippo effector Yap1 downstream of Fat4 to restrict heart growth. *Nat. Commun.* **8**, 14582. doi:10.1038/ncomms14582
- Saburi, S., Hester, I., Fischer, E., Pontoglio, M., Eremina, V., Gessler, M., Quaggin, S. E., Harrison, R., Mount, R. and McNeill, H. (2008). Loss of Fat4 disrupts PCP signaling and oriented cell division and leads to cystic kidney disease. *Nat. Genet.* **40**, 1010-1015. doi:10.1038/ng.179
- Saga, Y., Miyagawa-Tomita, S., Takagi, A., Kitajima, S., Miyazaki, J. and Inoue, T. (1999). MesP1 is expressed in the heart precursor cells and required for the formation of a single heart tube. *Development* **126**, 3437-3447.
- Schlegelmilch, K., Mohseni, M., Kirak, O., Pruszk, J., Rodriguez, J. R., Zhou, D., Kreger, B. T., Vasioukhin, V., Avruch, J., Brummelkamp, T. R. et al. (2011). Yap1 acts downstream of alpha-catenin to control epidermal proliferation. *Cell* **144**, 782-795. doi:10.1016/j.cell.2011.02.031
- Seo, E., Basu-Roy, U., Gunaratne, P. H., Coarfa, C., Lim, D.-S., Basilico, C. and Mansukhani, A. (2013). SOX2 regulates YAP1 to maintain stemness and determine cell fate in the osteo-adipo lineage. *Cell Reports* **3**, 2075-2087. doi:10.1016/j.celrep.2013.05.029
- Su, T., Bondar, T., Zhou, X., Zhang, C., He, H., Medzhitov, R. (2015). Two-signal requirement for growth-promoting function of Yap in hepatocytes. *Elife* **4**. doi:10.7554/eLife.02948
- Taylor, S. E., Shah, M. and Orriss, I. R. (2014). Generation of rodent and human osteoblasts. *Bonekey Rep.* **3**, 585. doi:10.1038/bonekey.2014.80
- Van Hateren, N. J., Das, R. M., Hautbergue, G. M., Borycki, A.-G., Placzek, M. and Wilson, S. A. (2011). FatJ acts via the Hippo mediator Yap1 to restrict the size of neural progenitor cell pools. *Development* **138**, 1893-1902. doi:10.1242/dev.064204
- Wang, F., Flanagan, J., Su, N., Wang, L. C., Bui, S., Nielson, A., Wu, X., Vo, H. T., Ma, X. J. and Luo, Y. (2012). RNAscope: a novel in situ RNA analysis platform for formalin-fixed, paraffin-embedded tissues. *The Journal of molecular diagnostics.* *J. Mol. Diagn.* **14**, 22-29. doi:10.1016/j.jmoldx.2011.08.002
- Westendorf, J. J., Zaidi, S. K., Cascino, J. E., Kahler, R., van Wijnen, A. J., Lian, J. B., Yoshida, M., Stein, G. S. and Li, X. (2002). Runx2 (*Cbfa1*, *AML-3*) interacts with histone deacetylase 6 and represses the p21(*CIP1/WAF1*) promoter. *Mol. Cell Biol.* **22**, 7982-7992. doi:10.1128/MCB.22.22.7982-7992.2002
- Xu, Y., Malladi, P., Zhou, D. and Longaker, M. T. (2007). Molecular and cellular characterization of mouse calvarial osteoblasts derived from neural crest and paraxial mesoderm. *Plast. Reconstr. Surg.* **120**, 1783-1795. doi:10.1097/01.prs.0000279491.48283.51
- Yang, J.-Y., Cho, S. W., An, J. H., Jung, J. Y., Kim, S. W., Kim, S. Y., Kim, J. E. and Shin, C. S. (2013). Osteoblast-targeted overexpression of TAZ increases bone mass in vivo. *PLoS ONE* **8**, e56585. doi:10.1371/journal.pone.0056585
- Young, M. F., Kerr, J. M., Termine, J. D., Wewer, U. M., Wang, M. G., McBride, O. W. and Fisher, L. W. (1990). cDNA cloning, mRNA distribution and heterogeneity, chromosomal location, and RFLP analysis of human osteopontin (OPN). *Genomics* **7**, 491-502. doi:10.1016/0888-7543(90)90191-V
- Yu, K., Xu, J., Liu, Z., Sosic, D., Shao, J., Olson, E. N., Towler, D. A. and Ornitz, D. M. (2003). Conditional inactivation of FGF receptor 2 reveals an essential role for FGF signaling in the regulation of osteoblast function and bone growth. *Development* **130**, 3063-3074. doi:10.1242/dev.00491
- Zaidi, S. K., Sullivan, A. J., Medina, R., Ito, Y., van Wijnen, A. J., Stein, J. L., Lian, J. B. and Stein, G. S. (2004). Tyrosine phosphorylation controls Runx2-mediated subnuclear targeting of YAP to repress transcription. *EMBO J.* **23**, 790-799. doi:10.1038/sj.emboj.7600073
- Zakaria, S., Mao, Y., Kuta, A., Ferreira de Sousa, C., Gaufo, G. O., McNeill, H., Hindges, R., Guthrie, S., Irvine, K. D. and Francis-West, P. H. (2014). Regulation of neuronal migration by dchs1-fat4 planar cell polarity. *Curr. Biol.* **24**, 1620-1627. doi:10.1016/j.cub.2014.05.067
- Zampino, G., Colosimo, C., Balducci, F., Mariotti, P., Serra, F., Scarano, G. and Mastroiacovo, P. (1994). Cerebro-facio-articular syndrome of Van Maldergem: confirmation of a new MR/MCA syndrome. *Clin. Genet.* **45**, 140-144. doi:10.1111/j.1399-0004.1994.tb04011.x
- Zhang, M., Xuan, S., Bouxsein, M. L., von Stechow, D., Akeno, N., Faugere, M. C., Malluche, H., Zhao, G., Rosen, C. J., Efstratiadis, A. et al. (2002). Osteoblast-specific knockout of the insulin-like growth factor (IGF) receptor gene reveals an essential role of IGF signaling in bone matrix mineralization. *J. Biol. Chem.* **277**, 44005-44012. doi:10.1074/jbc.M208265200